



Federal University of Bahia
Physics Post-Graduate Program

Relic Abundance of Monopoles via an Effective Field Theory

Pedro Carvalho Santos Brandão

Salvador

2022



Federal University of Bahia
Physics Post-Graduate Program

Pedro Carvalho Santos Brandão

**Relic Abundance of Monopoles via an Effective Field
Theory**

A dissertation submitted in partial fulfillment of the requirements for the degree of
MSc Physics

Supervisor: Prof. Dr. Luciano Melo Abreu

Salvador

2022

Agradecimentos/Acknowledgements

Primeiramente, agradeço aos meus pais, David e Christiane, por absolutamente tudo. Sou grato pelo amor, dedicação, amizade e pelo esforço perseverante em proporcionar tudo de melhor para os meus estudos. Para esses não há palavra que materialize tudo que sinto. Agradeço à minha irmã Luiza que na partilha do sonho acadêmico me fez valiosa companhia nas angústias e nas conquistas ao longo dessa etapa. Às minhas tias, em especial à minha madrinha e mãe Naize, pelo apoio e incentivo constante, sempre me fazendo sonhar mais alto. Ao meu tio Dourival pelo suporte e preocupação com meus estudos. Aos primos e primas, em especial Amon e Davi, pela parceria e conselhos. A minha vó Dora pelo carinho e cuidado desde sempre.

Agradeço a Lara por tantas conversas, pelo companheirismo e parceria nesses anos e sem a qual eu não teria a força para acreditar em mim. Agradeço aos meus amigos irmãos Caio, Walter, Ramon, Zau, Luís e Ítalo, a vida se torna muito mais alegre com vocês ao lado. Aos grandes amigos da UFBA, em especial José e Pietro, com os quais tive o privilégio de compartilhar boa parte da graduação. Agradeço a Rafael Menezes, Mena, pelas conversas lá no início do curso e por ter me convencido duas vezes a não desistir.

Agradeço a toda comunidade do Instituto de Física da UFBA. Aos bons professores que passaram pela minha formação, em especial ao professor Esdras, pelas conversas e reflexões que extrapolavam a física e me ensinaram o correto sentido dos estudos. Agradeço ao professor Luciano pelo exemplo de pesquisador, cientista e professor, que no sentido mais amplo da palavra, me orientou nessa caminhada. I would like to thank Professor Marc and Professor Pierre for the discussions and suggestions over this last year.

Agradeço imensamente à comunidade brasileira cuja contribuição me permitiu estudar em um universidade pública. Agradeço ao CNPq pela bolsa de mestrado.

“In the history of theoretical physics, the hypothesis about the possible existence of a magnetic monopole has no analogy. There is no other purely theoretical construction that has managed not only to survive, without any experimental evidence, in the course of more than a century, but has also remained the focus of intensive research by generations of physicists.”

– Yakov M. Shnir

Abstract

In this work, we revisit the thermal production and annihilation of monopoles and their relic abundance, exploiting the monopole phenomenology described by the effective field theory of monopole pair production via Drell-Yan process. We make use the vacuum cross sections for the Drell-Yan reactions to estimate the cross section averaged over the thermal distribution associated to other particles that constitute the hot medium where the monopoles propagate, in our case the early universe environment. Then, we use the thermally averaged cross sections as inputs to estimate the evolution of the Relic Abundance of monopoles following the freeze-out theory.

Keywords: monopoles, effective field theory, particle physics

Resumo

Neste trabalho, revisitamos a produção e aniquilação térmica de monopolos a fim de calcularmos sua Abundância Residual, explorando a fenomenologia descrita pela teoria de campo efetiva de produção do par monopolo/antimonopolo através do processo de Drell-Yan. Usamos as seções de choque do vácuo para estimar a média da seção de choque sobre a distribuição térmica associada a outras partículas que constituem o meio onde os monopolos se propagam, em nosso caso, o universo primitivo. Em seguida, utilizamos a média térmica das seções de choque para calcular e analisar a evolução da Abundância Residual de monopolos seguindo a teoria do "freeze-out".

Palavras-chave: teoria de campos efetiva, monopolos magnéticos, física de partículas

Contents

List of Tables	vii
List of Figures	viii
1 Introduction	1
2 The Effective Formalism	4
2.1 Effective formalism for monopole pair production and annihilation via Drell-Yan process	4
2.1.1 Scalar monopole	6
2.1.2 Fermionic monopole	8
2.1.3 The effective formalism for monopole pair annihilation via Drell-Yan process	9
2.2 Numerical Results	10
3 Thermally Averaged Cross Section	13
3.1 The thermal production and absorption of magnetic monopoles	13
3.1.1 Thermally averaged cross section for monopole pair production .	14
3.1.2 Thermally averaged cross section for monopole pair annihilation .	15
3.2 Plots and discussion	20
4 Relic Abundance	22
4.1 The Freeze-out Theory	22
4.2 Numerical results and discussion	27
5 Conclusions	29
Bibliography	30
Appendices	33
A Definitions	34
B Calculation of the invariant amplitudes and cross sections	37
B.1 Scalar monopole pair production	37

B.2 Fermionic monopole pair production	40
--------------------------------------------------	----

List of Tables

- 4.1 Magnitudes of temperature \tilde{T} and $\tilde{x} = m/\tilde{T}$ obtained from the condition in Eq. (4.13) for different values of the spin-zero monopole mass. 25
- 4.2 Magnitudes of temperature \tilde{T} and $\tilde{x} = m/\tilde{T}$ obtained from the condition in Eq. (4.13) for different values of the spin-half monopole mass. 25

List of Figures

2.1	Lepton pair production via Drell-Yan process	6
2.2	Total cross section for monopole -antimonopole pair production $q\bar{q} \rightarrow M\bar{M}$ as a function of the center-of-mass energy \sqrt{s} , with different values of the monopole mass M . Plots in the top and bottom panels describe spin-zero and spin-half monopoles, respectively.	10
2.3	Total cross section for monopole -antimonopole pair annihilation $M\bar{M} \rightarrow q\bar{q}$ as a function of the center-of-mass energy \sqrt{s} , with different values of the monopole mass M . Plots in the top and bottom panels describe spin-zero and spin-half monopoles, respectively.	11
3.1	<i>Top panel</i> the factor $F(T)$ as function of the temperature T for monopoles, considering the different masses studied in this work. <i>Bottom panel</i> the factor $F(T)$ as function of the temperature T for the up quark mass of 2.16×10^{-6} TeV.	15
3.2	Thermally averaged cross sections for monopole pair annihilation $M\bar{M} \rightarrow q\bar{q}$ as a function of $x = M/T$, with different values of the monopole mass M . Plots in the top and bottom panels describe spinless and spin-half monopoles, respectively.	20
4.1	Continuous variation of the stationary point \tilde{x} with the monopole mass according Eq. (4.13) obtained from the freeze-out theory. Plots in the top and bottom panels: cases of spin-zero and spin-half monopoles, respectively	26
4.2	The relic abundance $Y(x)$ for monopole as a function of $x = M/T$, according to Eq. (4.11), taking different values of the monopole mass M . Plots in the top and bottom panels: cases of spin-zero and spin-half monopoles, respectively.	27
4.3	The chemical potential for monopoles of spin 0 (Top panel) and spin 1/2 (Bottom panel) as a function of $x = M/T$, according to Eqs. (4.14) and (4.11), taking different values of the monopole mass M . Plots in the top and bottom panels: cases of spin 0 and 1/2, respectively.	28

Chapter 1

Introduction

It is a well-known fact that magnetic charges (or magnetic monopoles) have never been found in nature until now. Despite the lack of experimental evidences, since the complete formulation of the electromagnetism by Maxwell in the 19th century, the physicists have employed significant efforts not only to find them but also to include the magnetic charge in the modern framework of the theoretical physics. The idea that motivates generations of scientists in this attempt is based on a possible "symmetrization" of the Maxwell's equations, where monopoles could be include in the Gauss' law for the magnetic field playing the same role that electric charges play for electric fields. This concept of an "electric-magnetic duality" is widely used in the monopoles researches [1–3].

In the last century, the seminal paper by Dirac [4] fanned the flames of the discussion. He demonstrated that the existence of magnetic charge g implies in the quantisation of the electric charge q_e , according to the rule

$$q_e g = \frac{n}{2}, \quad (1.1)$$

for n integer and adopting the natural units ($c = \epsilon_0 = \hbar = 1$) which will be used in whole work from now on. Although the electric charge quantisation is one of the most fundamental fact of the quantum mechanics, why it happens remains without other explanation. It is interesting to note that the quantisation rule 1.1 is valid for particle that we can detect independently in nature. As there is no free quarks, i.e they are always confined into the hadrons, we can not use the Equation 1.1 to describe the electric charge fraction of these particles. Thus, a consistent quantum field theory for point-like monopoles emerged and many works in particle physics treat this hypothetical particle as a solution to some open questions in field theories and cosmology [5–9]. In the pioneering work of 't Hooft [6] and Polyakov [7] the existence of magnetic monopoles becomes essential in the grand unified theories (GUTs), which aims unify the electrodynamics, weak and strong interactions into one unified force. In that regard, searches for monopoles have been performed on particle accelerator such as Tevatron at Fermilab and the Large Hadron Collider (LHC) at CERN. The latter has the dedicated MoEDAL (Monopole and Exotics

Detector at the LHC) experiment deeply engaged in the searches for monopoles. Others monopoles searches could be found in Refs. [10–17].

However, for GUTs monopoles is expected a mass of about $10^{14} - 10^{16}$ GeV [3], which becomes its production impossible in the current particle colliders. Recently, the analysis of the MoEDAL trapping detector provided mass limits in the range 1500-3750 GeV for magnetic charges up to $5g_D$ for monopoles of spin 0, 1/2 and 1 [18]. With the current Run 3 of LHC, which will push the energy frontier further, the possibility of direct detection of a magnetic monopole is once more in the cards.

In addition, one of the consequences of GUTs is the prediction of a high actual abundance of monopoles (one per baryon), which exceeds the observation limit by a factor of 10^{12} [19–21]. The absence of observation of magnetic monopoles at the LHC up to this date, coupled with the non-observation of any relic monopoles argues that the relic monopole density is small.

As a deeper investigation of Baines et al's effective theory [22], we will investigate the behavior of this description in the early universe, since monopoles are stable particle and therefore monopoles produced in the early stages of the universe could be detected today. Along those lines, we examine the behavior of spinless and spin-half magnetic monopole pairs in a high-energy environment via the Drell-Yan process. The precise process by which monopoles would have been produced in the early universe depends on their details. In this work we analyze the cosmic relic abundance of magnetic monopoles from an effective field theory point of view based on the reference [23].

The Chapter 2 is dedicated to the construction of the effective formalism in order to find the cross sections of production, using [22] as main reference, and then the cross section of annihilation of monopoles. Both spin cases are analyzed, since the monopole spin remains a free parameter to be determined. Numerical calculations are performed and the results as well as the discussion can be found in the end of the chapter.

In Chapter 3 we use the results of the Chapter 2 as inputs to obtain the thermally averaged cross section for both production and annihilation of monopoles. The approach for the production follows the standard procedure described in [24] used in relativist heavy ion collisions, while for the annihilation process we follow the reference [25]. The graphs and discussion about the results are in the last section of the chapter.

In Chapter 4 we develop the calculations of the relic abundance following the reference [26] where the author present the "freeze-out" theory in the context of the WIMPS (Weakly interacting massive particles). We analyze the evolution of the abundance of monopoles divided into two stages: before and after the moment when the ratio of production and annihilation becomes stable. This point, as discussed in the chapter, is named "stationary point" and some consequences of this idea is analyzed as well. Finally, we obtain the evolution of the chemical potential. In the end, we present the findings and a discussion.

In Chapter 5 we summarize the general results obtained in this work and present some possible improvements in order to upgrade the future discussions. The notation as well as

the calculations of the invariant amplitudes and cross sections are detailed in Appendix A and B, respectively, at the end of this work.

Chapter 2

The Effective Formalism

In this chapter, we present the usual techniques of the Effective Field Theory applied to the monopoles based on the electric-magnetic duality. In section 2.1 and 2.2 we discuss the effective formalism to obtain the cross section of the monopole pair production and annihilation, respectively, considering both cases of spin-0 and 1/2. Then, in Section 2.3 we analyze the thermal production and absorption of monopoles. The respective thermally averaged cross sections are computed for both mentioned spin cases. In the end of the chapter we plot the total cross section for monopole-antimonopole pair production as a function of the center-of-mass energy \sqrt{s} for different values of the monopole mass M .

2.1 Effective formalism for monopole pair production and annihilation via Drell-Yan process

The first step in order to investigate the evolution of the abundance of monopole is to obtain its cross section of production. To this end, we use an effective U(1) gauge field theory described in Ref. [22], which considers the interaction of magnetically-charged fields with ordinary photons, based on the mentioned electric-magnetic duality. Unfortunately, the monopole mass and spin are still undetermined parameters, then, in this work, we will describe the interaction between the monopole of spin 0 and 1/2 with photons, performing the pertinent replacements in the Lagrangian density¹ of sQED (scalar quantum electrodynamics) and QED (quantum electrodynamics), respectively. With this considerations, we write [22]

$$\mathcal{L}^{(S=0)} = -\frac{1}{4}F^{\mu\nu}F_{\mu\nu} + (D^\mu\phi)^\dagger D_\mu\phi - M^2\phi^\dagger\phi, \quad (2.1)$$

¹In quantum field theory often the Lagrangian density is referred to as the Lagrangian. We will use this abbreviation in the text.

and

$$\mathcal{L}^{(S=1/2)} = -\frac{1}{4}F^{\mu\nu}F_{\mu\nu} + \bar{\psi}(i\gamma^\mu D_\mu - M)\psi, \quad (2.2)$$

where ϕ and ψ are the scalar and fermionic monopole fields, respectively; M is the monopole mass; $F_{\mu\nu} \equiv \partial_\mu A_\nu - \partial_\nu A_\mu$ is the field strength tensor; γ^μ are the Dirac matrices and $D_\mu \equiv \partial_\mu - igA_\mu$ the covariant derivative associated to the $U(1)$ photon gauge field A_μ , being g the monopole charge.

It is important to remark that many authors have used a monopole-velocity dependent magnetic charge $g(\beta)$, obtained under the replacement

$$g \rightarrow g\frac{v}{c} \equiv g\beta,$$

in order to interpret the data in the colliders searches for monopoles [28–33]. This conjecture comes from the non-relativistic electron-electron scattering motivated by the electric-magnetic duality as discussed in details in the reference [22]. Monopoles are hypothetical particles, so we can use both β -dependent and β -independent magnetic charge in our analyzes. As a first attempt, we consider the β -independent magnetic charge in this work.

After introducing the Lagrangians it is interesting to understand about the types of production and annihilation processes that we will consider. A typically Drell-Yan (DY) process consists in the quark/anti-quark pair annihilation creating a virtual photon which decays to a lepton/anti-lepton pair in the s-channel as we can see in Fig. (2.1). This mechanism has been used to investigate the lepton production in hadrons collisions e.g., relativistic heavy-ions collision. Since we are basing our work on the "electric-magnetic duality", it is reasonable to treat the monopole as a lepton in the same way as electron.

The high energy involved in this kind of collisions creates an environment very similar to the early universe shortly after the Big Bang and not for nothing it's often called "Little Bang". In both cases (Little and Big bang), before the hadronization, we have a primordial former of matter constituted by quarks and gluons forming a collective medium which flows as a relativistic hydrodynamics fluid, named Quark-Gluon Plasma (QGP), with remarkably low viscosity that can be treat as a perfect fluid. Only in the QGP phase we can see unconfined quarks and then the Drell-Yan process should play an even more important role. For more information about this subject one recommends the references [24, 34–36].

Following the development for the effective formalism, we analyze the Lagrangians (2.1) and (2.2) in order to compute the spin-averaged cross sections in the center of mass (CM) frame defined as usual:

$$\sigma_{ab \rightarrow cd}^{(S)}(s) = \frac{1}{64\pi^2 s} \frac{|\vec{p}_{cd}|}{|\vec{p}_{ab}|} \int d\Omega \sum_S |\mathcal{M}_{ab \rightarrow cd}^{(S)}(s, \theta)|^2, \quad (2.3)$$

where s is the the square of the centre of mass energy of the incoming particles; $\mathcal{M}_{ab \rightarrow cd}(s, \theta)$ represents the sum of the transition amplitudes of all processes contributing

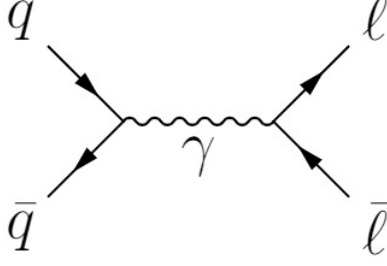


Figure 2.1: Lepton pair production via Drell-Yan process

to the interaction with $\overline{\sum}_S$ being the sum over the spins (or polarizations and colors, as needed) of the particles involved in the process, weighted by the degeneracy factors g_{1i} and g_{2i} of the two particles forming the initial state; $d\Omega$ is the infinitesimal solid angle and is defined in Appendix B. The three-momenta $|\vec{p}_{ab}|$ and $|\vec{p}_{cd}|$ are defined in terms of the Mandelstam variable s as

$$|\vec{p}_{ab}| = \frac{1}{2\sqrt{s}}[s^2 + (m_a^2 - m_b^2)^2 - 2s(m_a^2 + m_b^2)]^{1/2},$$

$$|\vec{p}_{cd}| = \frac{1}{2\sqrt{s}}[s^2 + (m_c^2 - m_d^2)^2 - 2s(m_c^2 + m_d^2)]^{1/2}. \quad (2.4)$$

2.1.1 Scalar monopole

On this section we will develop the effective formalism for spin-0 monopole production. Expanding out Eq. (2.1) we get

$$\mathcal{L}^{(S=0)} = -\frac{1}{4}F^{\mu\nu}F_{\mu\nu} - \phi^\dagger(\partial^2 + M^2)\phi - igA_\mu[(\partial^\mu\phi^\dagger)\phi - \phi^\dagger(\partial^\mu\phi)] + g^2A_\mu^2|\phi|^2. \quad (2.5)$$

In Eq. (2.5) we have the interaction terms in Lagrangian:

$$\mathcal{L}_{int1}^{(S=0)} = -igA_\mu[(\partial^\mu\phi^\dagger)\phi - \phi^\dagger(\partial^\mu\phi)], \quad (2.6)$$

$$\mathcal{L}_{int2}^{(S=0)} = g^2A_\mu^2|\phi|^2, \quad (2.7)$$

The Eq. (2.6) yields the vertex:

$$= -ig(p_1 + p_2)_\mu, \quad (2.8)$$

where $p_{1,2}$ and q_ρ are the monopole and photon four-momenta, respectively, and ϵ_λ the photon polarization.

The Eq. (2.7) provides:

$$= 2ig^2\eta_{\mu\nu}, \quad (2.9)$$

being $\eta^{\mu\nu}$ the Minkowski metric tensor with signature $(+, -, -, -)$. This diagram often is called "seagull vertex" and though it's a possible interaction allowed for the sQED theory it will not appear in the DY process. The diagram in Fig. (2.1) reveals only the three-point vertex. Taking the scalar monopole pair in the final state, we have the interaction with photons given by Eq. (2.8).

The quark-photon three-point vertex and the respective Feynman rule are:

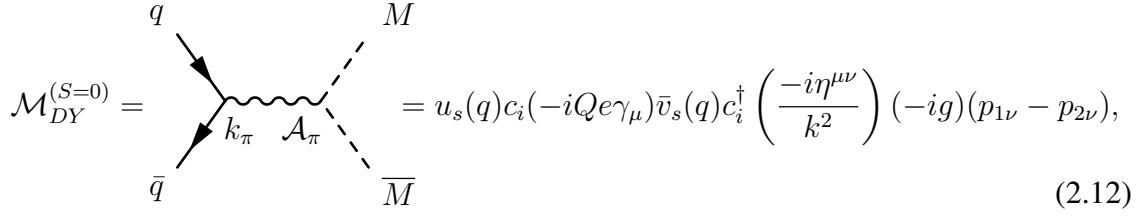
$$= -iQe\gamma^\mu, \quad (2.10)$$

e is the positron charge and Q is the electric charge fraction of quarks, $Q = 1/2, 3/2$. This interaction vertex could represent the coupling of any spin-1/2 fermion and a photon, including the fermionic monopole as we will see in the next section.

The last ingredient of our analyzes is the photon propagator that in the Feynman gauge is written as

$$= \frac{-i\eta^{\mu\nu}}{k^2}. \quad (2.11)$$

With Eq. (2.8), (2.10) and (2.11) the total matrix amplitude for the considered process is given by:



$$\mathcal{M}_{DY}^{(S=0)} = \text{Diagram} = u_s(q) c_i (-iQe\gamma_\mu) \bar{v}_s(q) c_i^\dagger \left(\frac{-i\eta^{\mu\nu}}{k^2} \right) (-ig)(p_{1\nu} - p_{2\nu}), \quad (2.12)$$

where $u_s(q)$ and $\bar{v}_s(q)$ are the quark/anti-quark spinors with dependence on the momentum q , respectively, and c_i is a vector associated with the colours of quarks. After some calculations detailed in Appendix B we can find the squared matrix amplitude averaged over quark spins and colors in terms of the Mandelstam variable s and the scattering angle θ as:

$$|\mathcal{M}_{DY}^{S=0}(s, \theta)|^2 = \frac{5}{3} e^2 g^2 \beta^2 [1 - \cos^2(\theta)], \quad (2.13)$$

where

$$\beta = \sqrt{1 - \frac{4M^2}{s}}, \quad (2.14)$$

is the monopole velocity. Using this results in Eq. (2.3), with Eq. (2.4), and integrating over the solid angle Ω we obtain the cross section for spin-0 monopole pair production:

$$\sigma_{q\bar{q} \rightarrow M\bar{M}}^{(S=0)}(s) = \frac{5\pi\alpha_g\alpha_e}{27s} \beta^3, \quad (2.15)$$

where α_g and α_e are the the magnetic and electric fine structure constant, respectively:

$$\begin{aligned} \alpha_g &= \frac{g^2}{4\pi}, \\ \alpha_e &= \frac{e^2}{4\pi}. \end{aligned} \quad (2.16)$$

2.1.2 Fermionic monopole

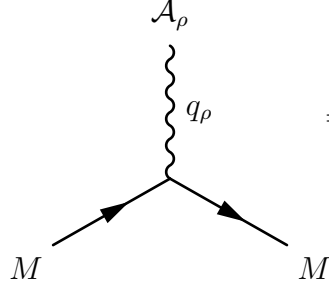
The pair production of spin-1/2 monopoles by Drell-Yan is analyzed in this section. Expanding out the Lagrangian (2.2) we have:

$$\mathcal{L}^{(S=1/2)} = -\frac{1}{4} F^{\mu\nu} F_{\mu\nu} + \bar{\psi}(i\gamma^\mu \partial - M)\psi + g\bar{\psi}\gamma^\mu\psi A_\mu, \quad (2.17)$$

where we have the interaction term in the same way we find in the standard QED under the replacement $e \rightarrow g$:

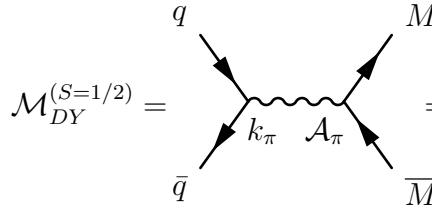
$$\mathcal{L}_{int}^{(S=1/2)} = g\bar{\psi}\gamma^\mu\psi A_\mu, \quad (2.18)$$

which yields a monopole-monopole-photon three-vertex with the Feynman rule:



$$= -ig\gamma^\nu. \quad (2.19)$$

The total matrix amplitude for spin-1/2 monopole pair production via DY can be calculated recovering the rules Eq. (2.10), (2.11) and using Eq. (2.19):



$$\mathcal{M}_{DY}^{(S=1/2)} = u_s(q)c_i(-iQe\gamma_\mu)\bar{v}_s(q)c_i^\dagger\left(\frac{-i\eta^{\mu\nu}}{k^2}\right)a_r(p)(-ig\gamma^\nu)\bar{b}_r(p), \quad (2.20)$$

being $a_r(p)$ and $\bar{b}_r(p)$ the spinors of monopoles with momentum p . As we can see in Appendix B:

$$|\mathcal{M}_{DY}^{S=1/2}(s, \theta)|^2 = \frac{e^2 g^2}{3} [2 - \beta^2(1 - \cos^2 \theta)]. \quad (2.21)$$

So, the cross section of the fermionic monopole pair production as function of the square of the centre-of-mass energy s is:

$$\sigma_{q\bar{q} \rightarrow MM}^{(S=1/2)}(s) = \frac{10\pi\beta\alpha_e\alpha_g}{27s}(3 - \beta^2). \quad (2.22)$$

2.1.3 The effective formalism for monopole pair annihilation via Drell-Yan process

After finding the cross section for the monopole production, we are able to obtain the cross section of the inverse process. We will input this quantity in the calculations of the thermally averaged cross section of absorption of monopoles in Chapter 3, that will be used to investigate the evolution of the relic abundance in Chapter 4. Then, the cross sections of the inverse process, in which the monopole pair is annihilated via Drell-Yan process, can be evaluated using the detailed balance relation [38], i.e.

$$\sigma_{cd \rightarrow ab}(s) = \frac{g_a g_b |\vec{p}_{ab}|^2}{g_c g_d |\vec{p}_{cd}|^2} \sigma_{ab \rightarrow cd}(s), \quad (2.23)$$

where $g_a = g_b = 2$ are the factors of degeneracy of spin of the quarks and g_c and g_d of the monopoles. For spin-0 monopoles $g_c = g_d = 1$ and for spin-1/2 monopoles $g_c = g_d = 2$. The three-momenta were defined in Eq. (2.4) and the cross section on right side was also calculated in Eq. (2.15) and (2.22). The graph can be seen in Fig.(2.3).

2.2 Numerical Results

The Fig. 2.2 shows the plots of the total cross sections as function of the center-of-mass energy obtained from Eq. (2.22) and (2.15) evaluated for different values of mass. We considered this range for the monopole mass motivated by the approach of Baines *et al's* [22].

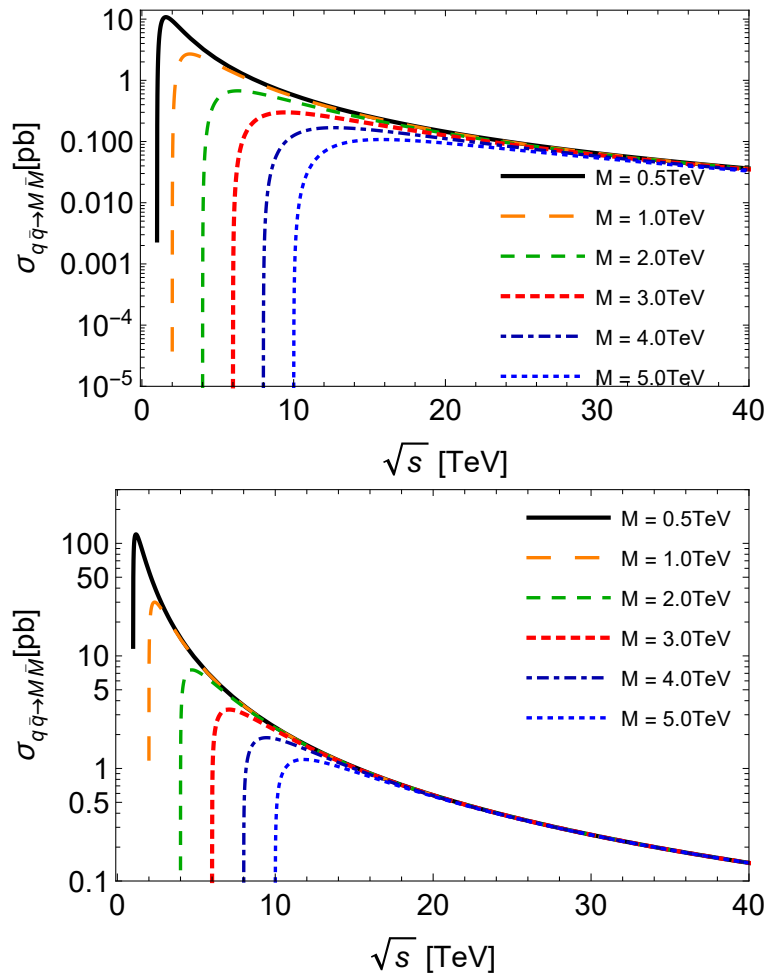


Figure 2.2: Total cross section for monopole -antimonopole pair production $q\bar{q} \rightarrow M\bar{M}$ as a function of the center-of-mass energy \sqrt{s} , with different values of the monopole mass M . Plots in the top and bottom panels describe spin-zero and spin-half monopoles, respectively.

The production cross sections are endothermic. Smaller values of mass provide higher

cross sections and the thresholds, i.e. \sqrt{s}_{min} , increases with M . One can observe from Fig. 2.2 that for both cases of spin 0 and $1/2$, immediately after the thresholds, the magnitude of the cross sections increases quickly reaching a maximum and as the CM energy increases, the cross section σ decreases for all processes, tending to the same behavior, almost indistinguishable at very high energies. At $\sqrt{s} \approx 15$ TeV, for example, this effective approach suggests cross sections with magnitudes of the order $\sim 10^{-1}$ pb and 1 pb for spin-0 and spin- $1/2$, respectively. For fermionic monopoles (bottom panel) the maximum occurs at much greater magnitudes, comparing with the scalar case (top panel), for the same value of mass.

Looking at the Fig. (2.3) we have plotted the inverse cross section for monopoles of spin 0 and $1/2$ as a functions of \sqrt{s} , considering different values of mass.

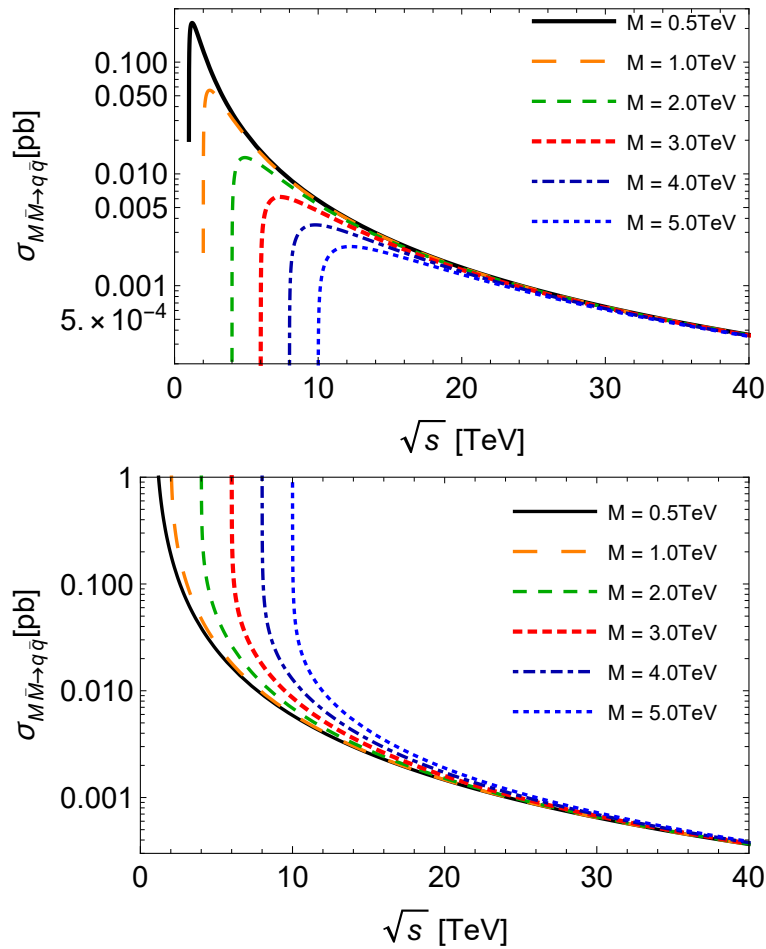


Figure 2.3: Total cross section for monopole -antimonopole pair annihilation $M\bar{M} \rightarrow q\bar{q}$ as a function of the center-of-mass energy \sqrt{s} , with different values of the monopole mass M . Plots in the top and bottom panels describe spin-zero and spin-half monopoles, respectively.

The Fig. (2.3) shows that the threshold increases with the mass, but here we have a different behavior near the thresholds. This is the case for spin-half monopoles: the curves for

$\sigma_{inv}^{(1/2)}$ become very large at their respective thresholds, and quickly decrease with larger \sqrt{s} . More interestingly, from moderate CM energies onward, these inverse cross sections become smaller than those for production reactions.

Note that for monopoles of spin $1/2$ we have an exothermic process which is expected once the mass of the monopole in the initial state is bigger than the quarks in the final state. Although, in the scalar case we have an unexpected endothermic process that could be understood as a consequence of the approximation $\beta_q \rightarrow 1$ in the calculation of the production cross sections discussed in Appendix B. In addition, at high values of \sqrt{s} in the both spin cases all curves converge to a specific value. Differently from the cross section of production, at $\sqrt{s} \approx 15$ TeV this effective approach suggests cross sections of absorption with magnitudes of the order $\sim 10^{-3}$ for both spin-zero and spin-half.

All this results will be used in the next section as input in the calculations of the thermally averaged cross sections.

Chapter 3

Thermally Averaged Cross Section

In this chapter we derive the thermally averaged cross section both for the production and annihilation process. We consider the Maxwell-Boltzmann distribution following the standard procedure of the thermal production of particles in a medium with high temperatures. In the end some plots and discussions are done.

3.1 The thermal production and absorption of magnetic monopoles

When we are treating with process which occur in environments where high energy (temperatures) is reached, the thermal effects cannot be neglected. In this scenario the medium plays an important role and has a great influence in the energy of reaction. In this work we are looking at the processes involving production and annihilation of monopoles in the early universe, before the photon decoupling, where the temperature in its initial stages could be hundreds, or even thousands, of MeV according the correspondence $t(s) \approx T^{-2}(\text{MeV})$ [39]. These extreme conditions of temperatures and density also could be found in the core of compact stellar objects, like neutron stars [40], and in ultra-relativistic heavy ion collisions [34]. Then, the processes discussed in Chapter 2, which led us to obtain the vacuum cross sections Eq.(2.15) and (2.22), and the formalism developed in this section can be applied in these scenarios as well.

Motivated by this, the next step is to calculate the quantity that includes the contribution of the temperature in the particle physics framework i.e. the thermally averaged cross section, which might be interpreted as the convolution of the vacuum cross section with thermal momentum distributions of the colliding particles.

3.1.1 Thermally averaged cross section for monopole pair production

Despite the previous discussion we introduce the cross section averaged over the thermal distribution for a reaction involving an initial two-particle state going into two final particles $ab \rightarrow cd$ [24]

$$\begin{aligned}
\langle \sigma_{ab \rightarrow cd} v_{ab} \rangle &= \frac{\int d^3 \mathbf{p}_a d^3 \mathbf{p}_b f_a(\mathbf{p}_a) f_b(\mathbf{p}_b) \sigma_{ab \rightarrow cd} v_{ab}}{\int d^3 \mathbf{p}_a d^3 \mathbf{p}_b f_a(\mathbf{p}_a) f_b(\mathbf{p}_b)} \\
&= \frac{1}{4x_a^2 K_2(x_a) x_b^2 K_2(x_b)} \int_{z_0}^{\infty} dz K_1(z) \\
&\quad \times \sigma(s = z^2 T^2) [z^2 - (x_a + x_b)^2] \\
&\quad [z^2 - (x_a - x_b)^2], \tag{3.1}
\end{aligned}$$

here v_{ab} is the relative velocity of the incoming particles and the function $f_i(\mathbf{p}_i)$ is the thermal distribution of particles of species i , which depends on the temperature T ; $x_i = m_i/T$ and $z_0 = \max(x_a + x_b, x_c + x_d)$ is the threshold i.e. the lowest energy allowed for the reaction in the centre-of-mass of the two colliding particles; K_1 and K_2 are the modified Bessel functions of the second kind.

In the case of thermal monopole production via $q\bar{q}$ annihilation, denoting the quark masses by m , we have from Eq. (3.1):

$$\langle \sigma_{q\bar{q} \rightarrow M\bar{M}} v_{q\bar{q}} \rangle^{(S)} = \frac{T^4}{4m^4 K_2^2(\frac{m}{T})} \int_{2M}^{\infty} dz K_1(z) \sigma_{q\bar{q} \rightarrow M\bar{M}}^{(S)}(s = z^2 T^2) \left[z^4 - \frac{4m^2 z^2}{T^2} \right]. \tag{3.2}$$

Looking at the equation above it is important to understand the behavior of the multiplicative factor before the integral. In order to clarify the analysis let's call this term of a function the temperature $F(T)$. The quark mass m is known and has a magnitude of $m \approx 10^{-6}$ TeV for lightest quark, reaching about $m \approx 10^{-3}$ TeV for the heavier quarks [41]. Thus we write

$$F(T) = \frac{T^4}{4m^4 K_2^2(\frac{m}{T})}. \tag{3.3}$$

It can be presumed that for small arguments (m/T) the Bessel function $K_2(m/T)$ increase quickly to very high values in denominator, that is the case for finite temperatures and the relatively small masses of the quarks. Consequently, $\langle \sigma_{ab \rightarrow cd} v_{ab} \rangle$ acquires very small magnitudes for monopole production processes with respect to the suppression ones; within the accuracy used in our numerical calculations, they become zero in most of the range of temperature considered. The behavior of the factor $F(T)$ in Eq. (3.3) can be seen in Fig 3.1 both for monopoles and up quark. Note that, the magnitude of the factor for up quarks is negligible comparing with the monopoles in the studied range of temperature. Because this we only consider in this work the thermally averaged cross section for the absorption of monopoles that will be presented in the next section.

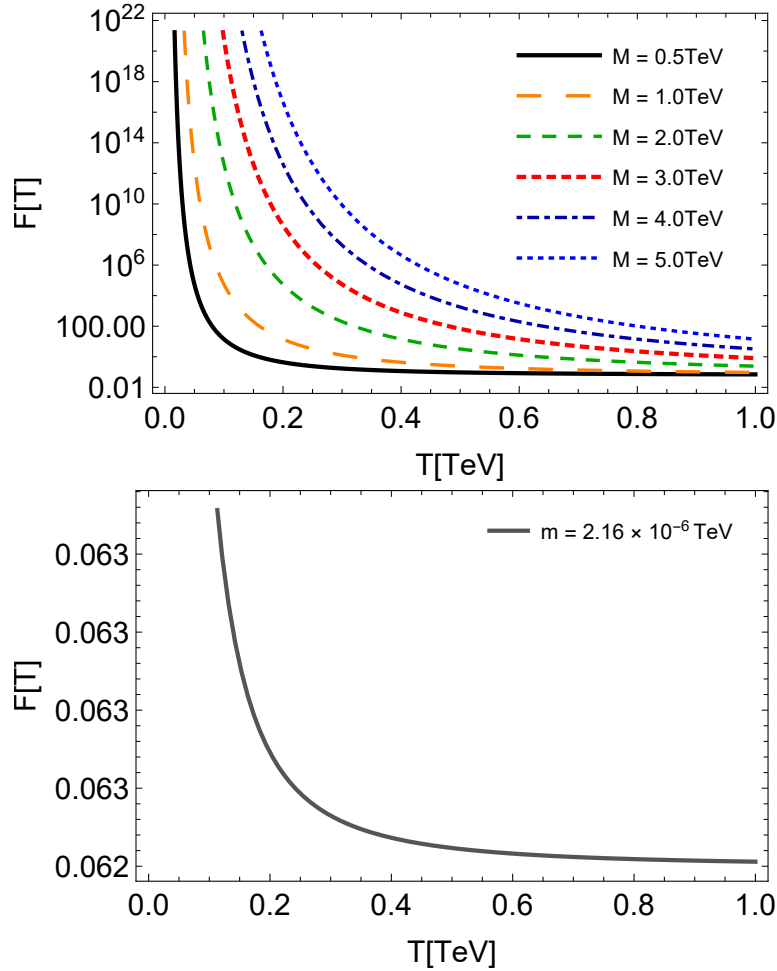


Figure 3.1: *Top panel* the factor $F(T)$ as function of the temperature T for monopoles, considering the different masses studied in this work. *Bottom panel* the factor $F(T)$ as function of the temperature T for the up quark mass of 2.16×10^{-6} TeV.

3.1.2 Thermally averaged cross section for monopole pair annihilation

In this section we will develop the thermally averaged annihilation cross section to determine the cosmic relic abundance of monopoles in Chapter 4. Our starting point is to assume that at high temperatures, which is the case in the early universe scenario, f_i in Eq. (3.1) is the equilibrium distribution function of Maxwell-Boltzmann. In that regard we write

$$f_i(E_i) \propto e^{-E_i/T}, \quad (3.4)$$

for particles at a temperature T in the cosmic comoving frame i.e. the coordinate system where the observer moves due solely to the expansion of the Universe. As discussed by

Gondolo and Gelmini [25] we can rewrite the standard Eq. (3.1) as:

$$\langle \sigma_{ab \rightarrow cd} v_{ab} \rangle = \frac{\int d^3 \mathbf{p}_a d^3 \mathbf{p}_b e^{-E_a/T} e^{-E_b/T} \sigma_{ab \rightarrow cd} v_{ab}}{\int d^3 \mathbf{p}_a d^3 \mathbf{p}_b e^{-E_a/T} e^{-E_b/T}}, \quad (3.5)$$

When we integrate a function which only depends on \mathbf{p} in the spherical coordinates we have for the momentum-space volume element $d^3 \mathbf{p} = p^2 \sin \theta dp d\theta d\phi$:

$$\begin{aligned} \int_{-\infty}^{+\infty} d^3 \mathbf{p} f(\mathbf{p}) &= \int_0^{2\pi} d\phi \int_{-1}^1 \sin \theta d\theta \int_0^\infty p^2 dp \\ &= (2\pi)(2) \int_0^\infty p^2 dp f(p), \end{aligned} \quad (3.6)$$

if $f(\mathbf{p}) = f(|\mathbf{p}|)$ follows

$$\int_0^\infty d^3 \mathbf{p} f(\mathbf{p}) = \int_0^\infty 2\pi p^2 dp f(p), \quad (3.7)$$

then

$$d^3 \mathbf{p}_a d^3 \mathbf{p}_b = 2\pi p_a^2 dp_a 2\pi p_b^2 dp_b d \cos \psi,$$

or in a more convenient form:

$$d^3 \mathbf{p}_a d^3 \mathbf{p}_b = 4\pi p_a^2 dp_a 4\pi p_b^2 dp_b \frac{1}{2} d \cos \psi, \quad (3.8)$$

where ψ is the angle between p_a and p_b ; $p_a = |\mathbf{p}_a|$ and $p_b = |\mathbf{p}_b|$. Now we use the relativistic relation between energy and momentum $E^2 = \mathbf{p}^2 + m^2$ from which we take the differential:

$$\begin{aligned} d(E^2) &= d(p^2) \\ 2EdE &= 2p dp \\ dp &= \frac{EdE}{p}, \end{aligned} \quad (3.9)$$

replacing Eq. (3.9) in Eq. (3.8) we get

$$\begin{aligned} d^3 \mathbf{p}_a d^3 \mathbf{p}_b &= 4\pi p_a^2 \frac{E_a dE_a}{p_a} 4\pi p_b^2 \frac{E_b dE_b}{p_b} \frac{1}{2} d \cos \psi \\ &= 4\pi p_a^2 E_a dE_a 4\pi p_b^2 E_b dE_b \frac{1}{2} d \cos \psi. \end{aligned} \quad (3.10)$$

Performing the change variable below

$$\begin{aligned} E_+ &= E_a + E_b \\ E_- &= E_a - E_b \\ s &= 2m^2 + 2E_a E_b - 2p_a p_b \cos \psi, \end{aligned} \quad (3.11)$$

the Eq. (3.10) becomes

$$d^3\mathbf{p}_a d^3\mathbf{p}_b = 2\pi^2 E_a E_b dE_+ dE_- ds. \quad (3.12)$$

In Eq. (3.10) the region of integration was given by the mass shell relation and it is given by $E_a > m$, $E_b > m$, and $|\cos \psi| \leq 1$. The new region of integration must be evaluated. Then, for E_+ we have from Eq. (3.11)

$$\begin{aligned} E_+^2 &= (E_a + E_b)^2 \\ &= p_a^2 + m^2 + 2E_a E_b + p_b^2 + m^2 \\ &= 2m^2 + 2E_a E_b + p_a^2 + p_b^2, \end{aligned} \quad (3.13)$$

where the particles a and b have the same mass and was used the relativistic relation between energy and momentum. Then, we have for the last two terms of Eq. (3.13)

$$p_a^2 + p_b^2 = (\mathbf{p}_a + \mathbf{p}_b)^2 - 2p_a p_b \cos \psi,$$

which provides for Eq. (3.13):

$$E_+^2 = 2m^2 + 2E_a E_b - 2p_a p_b \cos \psi + (\mathbf{p}_a + \mathbf{p}_b)^2,$$

using s given in Eq. (3.11) we find;

$$E_+ = \sqrt{s + (\mathbf{p}_a + \mathbf{p}_b)^2}, \quad (3.14)$$

and once $(\mathbf{p}_a + \mathbf{p}_b)^2 \geq 0$ we have for E_+ :

$$E_+ \geq \sqrt{s} \quad (3.15)$$

Using the same idea for E_- and s we can find:

$$|E_-| \leq \sqrt{1 - \frac{4m^2}{s}} \sqrt{E_+^2 - s}, \quad (3.16)$$

$$s \geq 4m^2. \quad (3.17)$$

Now we are able to perform the integration in Eq. (3.5) on the new variables. With the Eq. (3.12), let's start with the numerator:

$$\begin{aligned} \int d^3\mathbf{p}_a d^3\mathbf{p}_b e^{-E_a/T} e^{-E_b/T} \sigma_{ab \rightarrow cd} v_{ab} &= 2\pi^2 \int ds \sigma_{ab \rightarrow cd} v_{ab} E_a E_b e^{-E_+/T} \int dE_+ \int dE_- \\ &= 2\pi^2 \int dE_+ \int ds \sigma_{ab \rightarrow cd} v_{ab} E_a E_b \\ &\quad \times e^{-E_+/T} \sqrt{1 - \frac{4m^2}{s}} \sqrt{E_+^2 - s} \\ &= 2\pi^2 \int ds \sigma_{ab \rightarrow cd} v_{ab} E_a E_b \sqrt{1 - \frac{4m^2}{s}} \\ &\quad \times \int dE_+ e^{-E_+/T} \sqrt{E_+^2 - s}. \end{aligned} \quad (3.18)$$

Using the software *Wolfram Mathematica* we have for the given integration region of Eq. (3.15):

$$\int dE_+ e^{-E_+/T} \sqrt{E_+^2 - s} = T\sqrt{s} K_1\left(\frac{\sqrt{s}}{T}\right). \quad (3.19)$$

With this result the Eq. (3.18) becomes:

$$\int d^3\mathbf{p}_a d^3\mathbf{p}_b e^{-E_a/T} e^{-E_b/T} \sigma_{ab \rightarrow cd} v_{ab} = 2\pi^2 T \int ds \sigma_{ab \rightarrow cd} (s - 4m^2) \sqrt{s} K_1\left(\frac{\sqrt{s}}{T}\right), \quad (3.20)$$

for the denominator of Eq. (3.5) we follow a similar procedure and get

$$\int d^3\mathbf{p}_a d^3\mathbf{p}_b e^{-E_a/T} e^{-E_b/T} = \left[4\pi m^2 T K_2\left(\frac{m}{T}\right)\right]^2. \quad (3.21)$$

Then, replacing Eq. (3.20) and Eq. (3.21) in Eq. (3.5) and defining $m/T \equiv x$ we have the thermally averaged annihilation cross section which we will use as input into the relic abundance calculations in the next section given by

$$\langle \sigma v_{rel} \rangle = \frac{1}{8Tm^4 K_2^2(x)} \int_{4m^2}^{\infty} ds \frac{(s^2 - 4sm^2)}{\sqrt{s}} K_1\left(\frac{\sqrt{s}}{T}\right) \sigma(s). \quad (3.22)$$

Now we analyze this expression for the monopole case. Remembering that the cross section which appears in the right-hand side of the Eq. (3.22) is the annihilation cross section given by Eq. (2.23), we have for monopoles of spin 0 and 1/2:

$$\sigma_{M\bar{M} \rightarrow q\bar{q}}^{(S=0)}(s) = \binom{2}{1} \binom{2}{1} \frac{\sqrt{s}}{\sqrt{s - 4M^2}} \sigma_{q\bar{q} \rightarrow M\bar{M}}^{(S=0)}(s), \quad (3.23)$$

$$\sigma_{M\bar{M} \rightarrow q\bar{q}}^{(S=1/2)}(s) = \binom{2}{2} \binom{2}{2} \frac{\sqrt{s}}{\sqrt{s - 4M^2}} \sigma_{q\bar{q} \rightarrow M\bar{M}}^{(S=1/2)}(s). \quad (3.24)$$

The use of the cross section Eq. (3.24) into Eq. (3.22) allows to rewrite:

$$\begin{aligned} \langle \sigma_{M\bar{M} \rightarrow q\bar{q}} v_{M\bar{M}} \rangle^{(S=1/2)} &= \frac{5\pi\alpha_e\alpha_g}{36TM^4 K_2^2(x)} \int_{4M^2}^{\infty} ds \frac{(s^2 - 4sM^2)}{\sqrt{s}} K_1\left(\frac{\sqrt{s}}{T}\right) \frac{\sqrt{s}}{\sqrt{s - 4M^2}} \\ &\quad \times \frac{1}{s} \sqrt{1 - \frac{4M^2}{s}} \left[1 - \frac{1}{3} \left(1 - \frac{4M^2}{s}\right)\right]. \end{aligned}$$

Manipulating the integrand:

$$\begin{aligned} \langle \sigma_{M\bar{M} \rightarrow q\bar{q}} v_{M\bar{M}} \rangle^{(S=1/2)} &= \frac{5\pi\alpha_e\alpha_g}{18K_2^2(x)TM^3} \int_{4M^2}^{\infty} ds \sqrt{\frac{s}{4M^2} - 1} \sqrt{1 - \frac{4M^2}{s}} \left[\frac{2}{3} + \frac{1}{3} \frac{4M^2}{s}\right] \\ &\quad K_1\left(\frac{\sqrt{s}}{T}\right). \end{aligned}$$

According to [42] the next step is to perform the change of variable

$$y \longrightarrow \frac{s}{4M^2},$$

$$ds \longrightarrow 4M^2 dy,$$

then we have

$$\begin{aligned} \langle \sigma_{M\bar{M} \rightarrow q\bar{q}} v_{M\bar{M}} \rangle^{(S=1/2)} &= \frac{5\pi\alpha_e\alpha_g}{18TM^3K_2^2(x)} \int_1^\infty (4M^2) dy \sqrt{y-1} \sqrt{1-y^{-1}} \left[\frac{2}{3} + \frac{1}{3}y^{-1} \right] \\ &\times K_1(2x\sqrt{y}) \\ &= \langle \sigma_{v_{rel}} \rangle = \frac{10\pi\alpha_e\alpha_g x}{9M^2K_2^2(x)} \int_1^\infty dy (y-1)^{\frac{1}{2}} \frac{(y-1)^{\frac{1}{2}}}{y^{\frac{1}{2}}} \left[\frac{2}{3} + \frac{1}{3}y^{-1} \right] \\ &\times K_1(2x\sqrt{y}), \end{aligned}$$

and finally

$$\begin{aligned} \langle \sigma_{M\bar{M} \rightarrow q\bar{q}} v_{M\bar{M}} \rangle^{(S=1/2)} &= \frac{10\pi\alpha_e\alpha_g x}{9M^2K_2^2(x)} \int_1^\infty dy (y-1) \left[\frac{2}{3}y^{-\frac{1}{2}} + \frac{1}{3}y^{-\frac{3}{2}} \right] \\ &\times K_1(2x\sqrt{y}). \end{aligned} \quad (3.25)$$

We can rewrite in the form

$$\langle \sigma_{M\bar{M} \rightarrow q\bar{q}} v_{M\bar{M}} \rangle^{(S=1/2)} = \frac{10\pi\alpha_g\alpha_e x}{27M^2K_2^2(x)} \left[2I_{-\frac{1}{2}} - I_{-\frac{3}{2}} \right], \quad (3.26)$$

where the function I_p is given by

$$I_p = \int_1^\infty dy (y-1) y^p K_1(2x\sqrt{y}) .. \quad (3.27)$$

If we follow the same procedure for spin-0, using the pertinent quantities we find:

$$\langle \sigma_{M\bar{M} \rightarrow q\bar{q}} v_{M\bar{M}} \rangle^{(S=0)} = \frac{20\pi\alpha_g\alpha_e x}{27M^2K_2^2(x)} \left[I_{-\frac{1}{2}} + I_{-\frac{3}{2}} \right]. \quad (3.28)$$

According [42] this approach is valid when the masses of the particles in the final state are much smaller than those in the initial state. Then, we assume $m_q = m_{\bar{q}} = 0$ and $m_M = m_{\bar{M}} = M$.

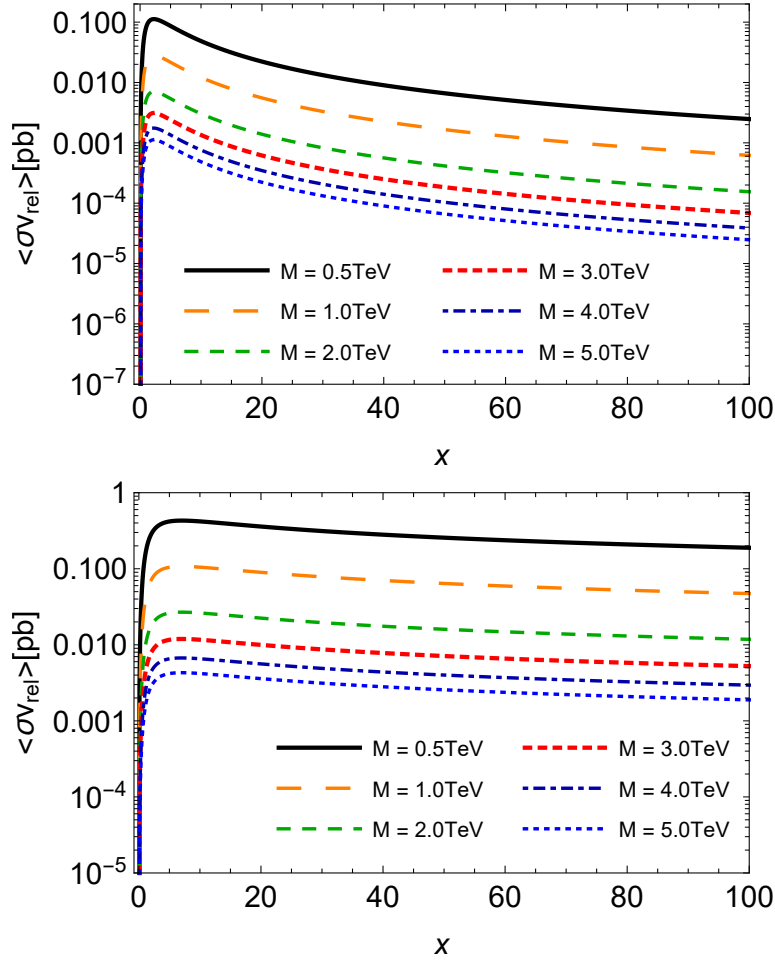


Figure 3.2: Thermally averaged cross sections for monopole pair annihilation $M\bar{M} \rightarrow q\bar{q}$ as a function of $x = M/T$, with different values of the monopole mass M . Plots in the top and bottom panels describe spinless and spin-half monopoles, respectively.

3.2 Plots and discussion

The Fig. 3.2 show the thermally averaged cross section for the annihilation of monopoles of spin 0 and 1/2 as function of the parameter $x = M/T$ considering different values of mass.

Here again, higher magnitudes are achieved for reactions involving monopoles with smaller masses, and as the temperature decreases (i.e. the variable x augments) this difference is kept nearly constant within the considered range of x . Also, these respective magnitudes are similar for both spin-zero and spin-half monopoles in the region near $x \sim 2$. We point out that, as we increase x , $\langle \sigma_{M\bar{M} \rightarrow q\bar{q}} v_{M\bar{M}} \rangle$ for spin-zero drops faster than that for spin-half; indeed, the latter suffers just a very slight decrease in the studied range. In other words, the decreasing of temperature engenders a rate of annihilation for scalar monopoles smaller than the one for fermionic monopoles.

Note that the difference between the magnitudes of thermally averaged cross sections for the annihilation reactions and the production reactions might, in principle, play an important role in the search for monopoles in the evolution of the monopole abundance of cosmic origin and in future heavy-ion colliders.

Equipped with this thermally averaged cross section, we will investigate the evolution of the abundance in the next section.

Chapter 4

Relic Abundance

In this chapter we will use the thermally averaged cross sections calculated in the Chapter 3 in order to obtain the Relic Abundance of monopoles by freeze-out theory. First we discuss about the concept of freeze-out and then develop the standard Boltzmann rate equation for the evolution of the particle number aiming to get the differential equation for the Relic Abundance $Y(x)$. After we examine some properties of $Y(x)$ and determine a piecewise function for this quantity which yields an especial point named "stationary point", \tilde{x} , where the behavior of $Y(x)$ is ruled by different functions after and before it. Finally, we discuss about the chemical potential and its evolution for different masses of monopoles. We obtain the numerical results for all this quantities and in the end of the chapter we plot and analyze the results.

4.1 The Freeze-out Theory

The last sections provided us the necessary tools to compute the Relic Abundance of monopoles in the early universe environment. Here we will make use of the so-called "freeze-out theory" [26] which is built from the standard hot Big-bang model, or as it is also called, Friedmann–Robertson–Walker (FRW) cosmological model, where is assumed a homogeneous and isotropic expanding universe. The concept of isotropy means that there is no special direction i.e there is no difference in the structure of the Universe as you look in different places. The homogeneity is the assumption that the averaged density of matter in the universe is about the same on large scales [43]. The most fundamental feature of this model is the description of the expansion of the universe [44]. This idea refers to the fact that, after the Big-bang, the universe starts an expansion of space which increases all distances between any two points and it plays an important role in the freeze-out theory.

In the first stages of its formation, precisely in the "radiation-dominated era", the universe was extremely hot and dense, and then an enormous amount of event of creation and destruction of all kind of particles was occurred at very high rate. Because that any particle could exist for a long time. As the universe expanded and cooled down, it reaches a specific temperature, the "freeze-out temperature", where the production and annihilation rates of the stable particles become uniform. After this time (or temperature¹), named stationary point, it remains a residual number of particle i.e. the Relic Abundance. This framework has been employed in several scenarios, like in the analysis of dark matter. We label this stationary point by $x = \tilde{x}$, it depends on the mass (according to the definition $x = M/T$) and the interactions.

We start from the Boltzmann rate equation that governs the evolution of the relic number density [45]:

$$\dot{n} + 3Hn = - \langle \sigma_{M\bar{M} \rightarrow q\bar{q}} v_{M\bar{M}} \rangle (n^2 - n_0^2), \quad (4.1)$$

where $\langle \sigma_{ann} v \rangle$ is the thermally averaged cross section for the annihilation process (i.e. $M\bar{M} \rightarrow q\bar{q}$ in our case); n_0 is the number density in the thermal equilibrium; H is the Hubble parameter $H = \dot{R}/R = \sqrt{8\pi G\rho/3}$ in the FRW cosmology, with $G = 1/M_P^2$ being the cosmological constant ($M_P = 1.22 \times 10^{16}$ TeV is the Planck mass), where R is the cosmic scale factor, and $\rho = \pi^2 g_\rho T^4/30$ the total energy density of the universe (g_ρ counts the relativistic degrees of freedom contributing to the energy density). The expansion of the universe is an adiabatic process, so the entropy per comoving volume $S = R^3 s$ is conserved. Here $s = (2\pi^2/45)g_s T^3$ is the entropy density with g_s being the relativistic degrees of freedom associated to the the total entropy density. Dividing Eq. (4.1) by S and using the constant H in terms of R , it follows

$$\frac{\dot{n}}{R^3 s} + 3 \frac{\dot{R}}{R} \frac{n}{R^3 s} = - \frac{1}{R^3 s} \langle \sigma_{M\bar{M} \rightarrow q\bar{q}} v_{M\bar{M}} \rangle (n^2 - n_0^2). \quad (4.2)$$

Note that the time derivative of S is:

$$\dot{S} = 3R^2 \dot{R} s + R^3 \dot{s}, \quad (4.3)$$

once $\dot{S} = 0$, Eq. (4.3) provides

$$\frac{\dot{s}}{s} = -3 \frac{\dot{R}}{R} = -3H$$

replacing it in Eq. (4.2) and developing the right side to a convenient form, we get:

$$\frac{dn}{dt} \frac{1}{s} - \frac{\dot{s}}{s^2} n = -s \langle \sigma_{M\bar{M} \rightarrow q\bar{q}} v_{M\bar{M}} \rangle \left[\left(\frac{n}{s} \right)^2 - \left(\frac{n_0}{s} \right)^2 \right]. \quad (4.4)$$

The left hand side can be rewrite using:

$$\frac{d}{dt} \left(\frac{n}{s} \right) = \frac{dn}{dt} \frac{1}{s} - \frac{\dot{s}}{s^2} n. \quad (4.5)$$

¹Since our interest is to analyze the thermal production of monopoles, the temperature is most useful to being used as the evolution parameter of the system instead the time.

It is useful to use the ratio of the number of particles to the entropy $Y = n/s$. So replacing Eq. (4.5) in Eq. (4.4):

$$\frac{dY}{dt} = -s \langle \sigma_{M\bar{M} \rightarrow q\bar{q}} v_{M\bar{M}} \rangle (Y^2 - Y_0^2) \quad (4.6)$$

Thereafter, the variable is changed by employing the correspondence $d/dt \rightarrow Hx d/dx$, enabling one to rewrite the rate equation for the relic abundance as function of x in the form,

$$\frac{dY}{dx} = \frac{C}{x^2} \langle \sigma_{M\bar{M} \rightarrow q\bar{q}} v_{M\bar{M}} \rangle (Y_0^2 - Y^2), \quad (4.7)$$

where

$$Y_0 = 45/(4\pi^4)(g/g_s)x^2 K_2(x), \quad (4.8)$$

is the initial equilibrium abundance ($g = 1$ or 2 , for scalar or fermionic monopoles, respectively), and $C = \sqrt{\frac{\pi}{45}} M_P M \sqrt{g_*}$, with

$$\sqrt{g_*} = \frac{g_s}{\sqrt{g_\rho}} \left(1 + \frac{T}{3} \frac{d(\ln g_s)}{dT} \right), \quad (4.9)$$

depending on the relativistic degrees of freedom g_ρ and g_s .

An important remark to do here is that the Eq. (4.7) describe the evolution of the abundance after the stationary point \tilde{x} . To analyze epochs before \tilde{x} we have the function:

$$Y_1(x) = \sqrt{Y_0^2 - \frac{x^2}{C \langle \sigma_{M\bar{M} \rightarrow q\bar{q}} v_{M\bar{M}} \rangle} \frac{dY_0}{dx}}, \quad (4.10)$$

The evolution can be studied into two stages: at early times where we have Eq. (4.10) governing the abundance until the point \tilde{x} , and at later times with Eq.(4.7) that we will denote by $Y_2(x)$. Then, the true relic abundance $Y(x)$ can be defined by the piecewise function

$$Y(x) = \begin{cases} Y_1(x), & x \leq \tilde{x}, \\ Y_2(x), & x \geq \tilde{x}, \end{cases} \quad (4.11)$$

The next step is to discuss how to determine the stationary point \tilde{x} . For this purpose we define the difference $\Delta = Y - Y_0$, the amount of abundance distant from equilibrium. Then, the matching point between the solutions in the two regions of x can be estimated by means of $\Delta(\tilde{x}) = cY_0(\tilde{x})$, where c is a numerical factor determined by the numerical solution of the rate equation. Different values for c have been proposed in the literature in distinct physical scenarios Ref. [26]. As a first attempt, here we adopt the condition $\Delta(\tilde{x}) = Y_0(\tilde{x})$, yielding $Y_2(\tilde{x}) = Y_1(\tilde{x}) = 2Y_0(\tilde{x})$. Rewriting $Y_1(x)$ in Eq. (4.10) in the form $Y_1(x) \equiv (1 + \delta(x))Y_0(x)$, where

$$\delta(x) = \sqrt{1 - \frac{x^2}{C \langle \sigma_{M\bar{M} \rightarrow q\bar{q}} v_{M\bar{M}} \rangle Y_0^2} \frac{dY_0}{dx}} - 1, \quad (4.12)$$

we obtain, for the assumed condition above, $\delta(\tilde{x}) = 1$, which is equivalent to

$$-\frac{1}{Y_0} \frac{dY_0}{dx} \Big|_{x=\tilde{x}} = \left[3 \frac{C}{x^2} \langle \sigma_{M\bar{M} \rightarrow q\bar{q}} v_{M\bar{M}} \rangle Y_0 \right]_{x=\tilde{x}}. \quad (4.13)$$

Finding the root of the Eq. (4.13) we obtain different values for \tilde{x} depending on the monopole mass as we can see in Table 4.1. According to this result, the freeze-out temperature \tilde{T} increases with the mass, which means that heavier monopoles should be produced in earlier stages of the universe. It is important to remark that, after performing numerical calculation to find the roots of Eq. (4.13), \tilde{x} does not present a sensible difference for both spin cases, although this dependence appears in Eq. (4.13) due to the cross section and the degeneracy factor g . This result suggests that spin-zero and spin-half would have left a relic abundance at the same moment of evolution of the universe, once the same temperature \tilde{T} is obtained for both spin cases. We also include the stationary point evaluated for a mass with a magnitude of 10^4 TeV, which has been related as an upper limit imposed by the nucleosynthesis constraints on the abundance of relic monopoles [3, 46]. The Fig. 4.1 shows the continuous variation of \tilde{x} in the studied range.

Table 4.1: Magnitudes of temperature \tilde{T} and $\tilde{x} = m/\tilde{T}$ obtained from the condition in Eq. (4.13) for different values of the spin-zero monopole mass.

Mass (TeV)	\tilde{T} (TeV)	\tilde{x}
0.5	0.02	29.42
1.0	0.03	28.75
2.0	0.07	28.08
3.0	0.11	27.69
4.0	0.15	27.41
5.0	0.18	27.20
10^4	486.38	20.56

Table 4.2: Magnitudes of temperature \tilde{T} and $\tilde{x} = m/\tilde{T}$ obtained from the condition in Eq. (4.13) for different values of the spin-half monopole mass.

Mass (TeV)	\tilde{T} (TeV)	\tilde{x}
0.5	0.02	29.82
1.0	0.03	29.15
2.0	0.07	28.49
3.0	0.11	28.09
4.0	0.14	27.82
5.0	0.18	27.60
10^4	492.61	20.30

We are adopting the idea that in the first stages the thermal (and chemical) equilibrium holds. As the universe is expanding and cooling, the particles, in our case the monopoles, start an evolution to a nonzero chemical potential. It is related to the ‘‘affinity’’, defined as $\mathcal{A} = -\sum_i \nu_i \mu_i$, where μ_i are the chemical potentials of the species of type i , and ν_i

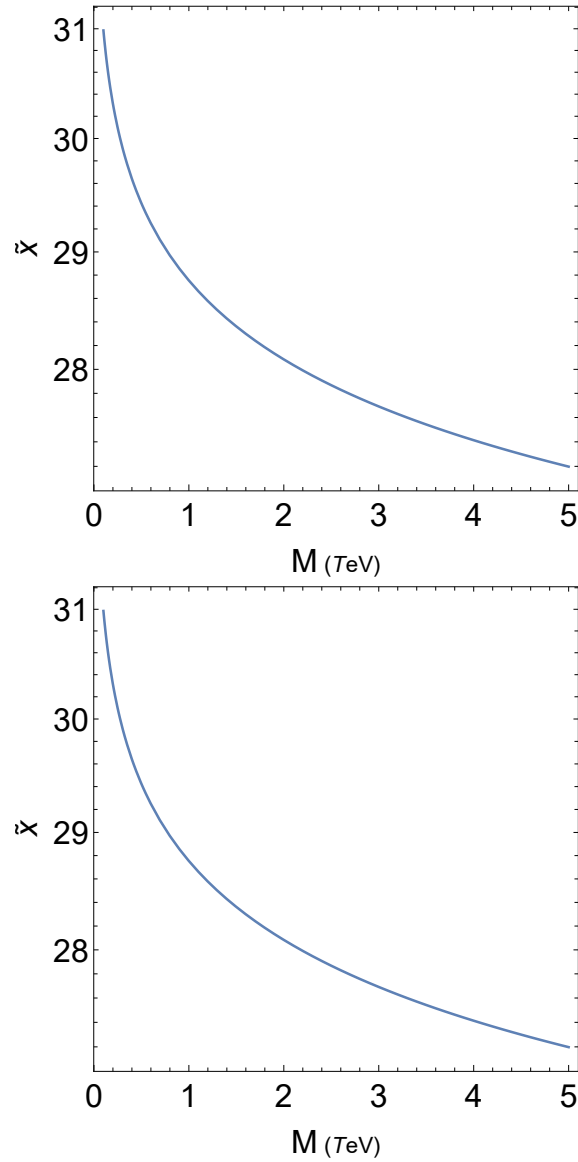


Figure 4.1: Continuous variation of the stationary point \tilde{x} with the monopole mass according Eq. (4.13) obtained from the freeze-out theory. Plots in the top and bottom panels: cases of spin-zero and spin-half monopoles, respectively

are the stoichiometric coefficients, which are assumed to be negative for monopoles and antimonopoles, yielding $\mathcal{A} = 2\mu$ [26]. If we assume that it is related to the *log* of the ratio between the production and annihilation rates, i.e. the two terms in the right-hand side of the rate equation in (4.1), then one can write the chemical potential as

$$\mu = \frac{M}{x} \ln \left(\frac{Y}{Y_0} \right). \quad (4.14)$$

4.2 Numerical results and discussion

Now we are able to discuss about the results obtained above. In the Fig. 4.2 we have the plot of the Relic Abundance as function of the parameter $x = M/T$ given in Eq. (4.11). First of all, looking at the Fig. 4.2 we can see that before the stationary point, the abun-

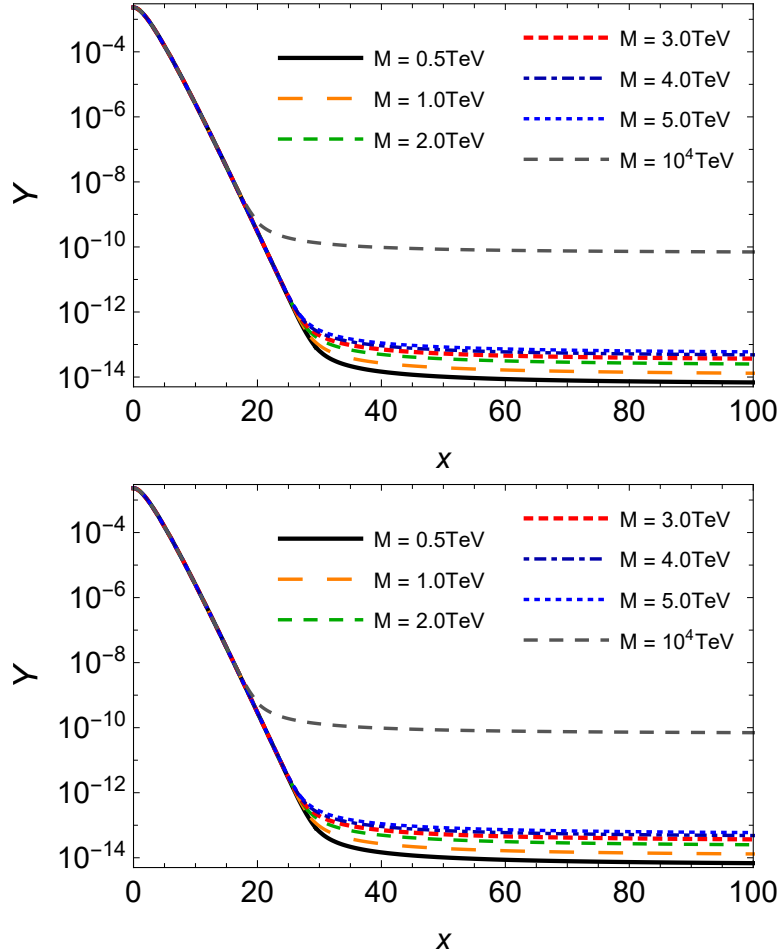


Figure 4.2: The relic abundance $Y(x)$ for monopole as a function of $x = M/T$, according to Eq. (4.11), taking different values of the monopole mass M . Plots in the top and bottom panels: cases of spin-zero and spin-half monopoles, respectively.

dance evolves in a very similar way for all values of the monopole mass in both spin cases. After \tilde{x} there is reasonable difference in the abundance for each value of mass. The abundance of monopoles increases directly with the monopole mass. Comparing the abundance of monopoles with $M = 0.5$ TeV and $M = 5.0$ TeV we have a difference of one order of magnitude in their relic abundance. It can be seen as a theoretical evidence that heavy monopoles are more stable than light monopoles. The results suggest that the abundance does not behave differently for spin-zero and spin-half relic monopoles.

From the quantitative point of view, the values estimated for the relic abundance are clearly high, in view of the effective formalism and the magnitudes of the couplings and

quantities taken. In that regard, the density of relic monopoles is naturally modified for different set of values for the relevant parameters, e.g. $g_D, \sqrt{g_*}, \sqrt{g_s}$ and so on. Clearly, more accurate analyses are needed to improve the present investigation such as, for example, the impact of our distinct assumptions on the values of the relevant parameters, the inclusion of other variables of interest (e.g. magnetic background), and so on. We postpone them for future discussions.

In addition, we can see the chemical potential as function of x for both spin cases in Fig.4.3, according to Eqs. (4.14) and (4.11), for different values of M . Since a non-zero chemical potential means a process out of chemical equilibrium, we see that at earlier stages of the universe, μ increases by several orders of magnitude, but as x increases and the rate in the definition of μ decreases, this yields a moderate growth. At larger x , i.e. smaller temperatures, this rate is very small, and μ saturates to an asymptotic value and the abundance tends to be constant. Interestingly, the asymptotic value is just the monopole mass, similarly to the findings in Ref. [26].

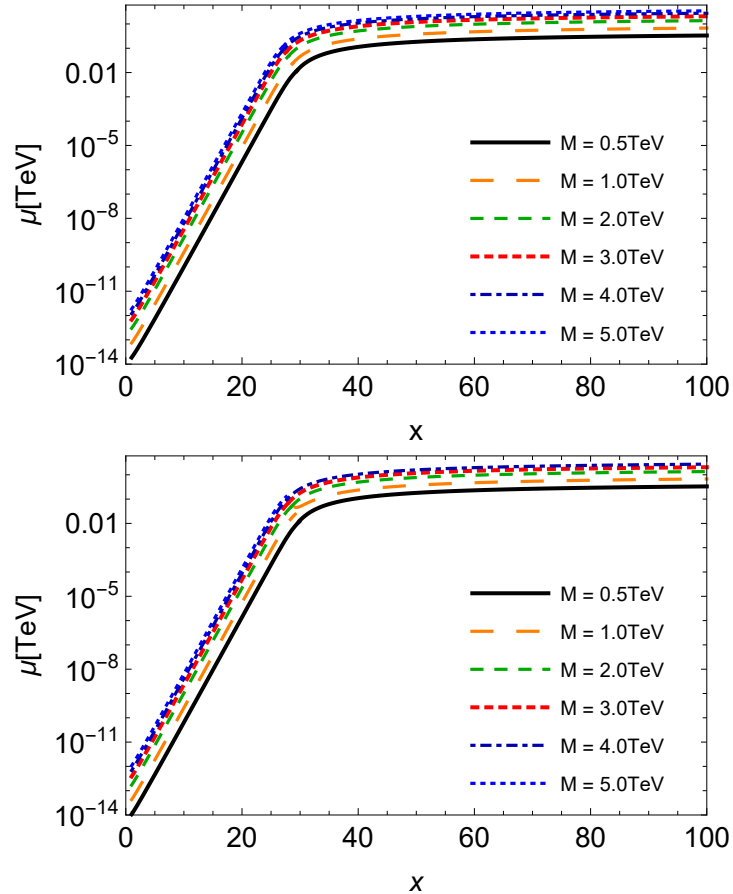


Figure 4.3: The chemical potential for monopoles of spin 0 (Top panel) and spin 1/2 (Bottom panel) as a function of $x = M/T$, according to Eqs. (4.14) and (4.11), taking different values of the monopole mass M . Plots in the top and bottom panels: cases of spin 0 and 1/2, respectively.

Chapter 5

Conclusions

In this work we have analyzed the relic abundance of monopoles, in the early universe scenario, using the mechanism of the freeze-out theory proposed by [26]. In this regard, we have used the effective field theory, presented by Baines *et al*, in order to find the vacuum cross sections for the Drell-Yan reactions, which we have used as input to estimate the thermally averaged cross sections. Once the spin and mass of monopoles remain a free parameters, we have considered the case of the scalar and fermionic monopole for all quantities calculated. In the chosen range of mass, our results showed that the thermally averaged cross sections for the pair production are highly suppressed while, at higher temperatures, the cross sections for the annihilation of lighter pairs reach larger values. In addition, the rate of annihilation for scalar monopoles is smaller than for fermionic monopoles, which can be understood as a theoretical evidence of a more stability for heavy monopoles of spin-0. This might be relevant in the search for monopoles in future heavy-ion colliders and of cosmic origin.

Then, we describe the evolution of the relic abundance of monopoles using the thermally averaged cross sections as input. Our results endorse the previous assertion, once larger mass of monopoles produce higher values of the relic abundance. Besides, heavier monopoles showed to reach the equilibrium at higher temperatures than the lightest, implying in the fact that, as the mass of monopole increases, it left a relic abundance in earlier stage of the universe. No difference for scalar and fermionic monopole was found in their abundance.

To conclude, we emphasize that our general objective was to study the implications of the effective field theory of Ref. [22] on some aspects of the monopole phenomenology. Clearly, more accurate analyses are needed to improve the present investigation such as, for example, the impact of our distinct assumptions on the values of the relevant parameters, the inclusion of other variables of interest (e.g. magnetic background), and so on. We postpone them for future discussions.

Bibliography

- [1] Y. M. Shnir, *Magnetic Monopoles*. Springer Berlin, 2005.
- [2] J. Preskill, “Magnetic monopoles”, *Ann. Rev. Nucl. Part. Sci.* 34:461-530., 1984.
- [3] N. E. Mavromatos and V.A.Mitsou, “Magnetic monopoles revisited: Models and searches at colliders and in the cosmos”, *Int. J. Mod. Phys. A no.23*, 2020.
- [4] P. A. M. Dirac, “Quantised singularities in the electromagnetic field.”, *Proc. R. Soc. London A 1 3 3 : 60.*, 1931.
- [5] J. S. Schwinger, “A magnetic model of matter”, *Science*, vol. 165, 1969.
- [6] G. Hooft, “Magnetic monopoles in unified gauge theories”, *Nuclear Physics B*, vol. 79, no. 2, pp. 276–284, 1974, ISSN: 0550-3213.
- [7] A. Polyakov, “Magnetic monopoles revisited: Models and searches at colliders and in the cosmos”, *JETP Lett.*, vol. 20, 1974).
- [8] Y. Cho and D. Maison, “Monopole configuration in weinberg-salam model”, *Phys. Lett. B*, vol. 391, 1997).
- [9] Y. Cho, K. Kim, and J. Yoon, “Finite energy electroweak dyon”, *Eur. Phys. J. C*, vol. 75, 2015).
- [10] ATLAS Collaboration, “Search for magnetic monopoles and stable high-charge objects in 13 tev proton-proton collisions with the atlas detector”, *Phys. Rev. Lett.* 124, 031802, 2020.
- [11] B. Acharya and others et al. (MoEDAL Collaboration), “The physics programme of the moedal experiment at the lhc”, *International Journal of Modern Physics A Vol. 29, No. 23, 1430050*, 2014.
- [12] IceCube Collaboration, “Search for relativistic magnetic monopoles with eight years of icecube data”, *Phys. Rev. Lett.* 128, 051101, 2022.
- [13] —, “Searches for relativistic magnetic monopoles in icecube”, *The European Physical Journal C volume 76*, 2016.
- [14] —, “Search for non-relativistic magnetic monopoles with icecube”, *The European Physical Journal C volume 74*, 2014.
- [15] Super-Kamiokande Collaboration, “Search for gut monopoles at super-kamiokande”, *Astroparticle Physics* 36, 2012.

- [16] ANITA-II Collaboration, “Ultrarelativistic magnetic monopole search with the anita-ii balloon-borne radio interferometer”, *Phys. Rev. D* 83, 023513, 2011.
- [17] NOvA Collaboration, “Search for slow magnetic monopoles with the nova detector on the surface”, *Phys. Rev. D* 103, 012007, 2021.
- [18] B. Acharya and others et al. (MoEDAL Collaboration), “Magnetic monopole search with the full moedal trapping detector in 13 tev pp collisions interpreted in photon-fusion and drell-yan production”, *Phys. Rev. Lett.* 123, 2019.
- [19] M. S. Turner, “Thermal production of superheavy monopoles in the early universe”, *Physics Letters Volume 115B, number 2*, 1982.
- [20] J. Preskill, “Cosmological production of superheavy magnetic monopoles”, *Phys. Rev. Lett.* 43, 1979.
- [21] Y. Zel’dovich and M. Khlopov, “On the concentration of relic magnetic monopoles in the universe”, *Phys. Lett.* 79B, 1979.
- [22] S. Baines, N. E. Mavromatos, V. A. Mitsou, J. L. Pinfold, and A. Santra, “Monopole production via photon fusion and drell-yan processes: Madgraph implementation and perturbativity via velocity-dependent coupling and magnetic moment as novel features”, *Eur. Phys. J. C*, vol. 78:966, 2018.
- [23] L. M. Abreu, P. C. S. Brandão, M. de Montigny, and P.-P. A. Ouimet, “An effective field theory treatment of the production and annihilation of magnetic monopoles and their relic abundance”, *arXiv:2206.11394 [hep-ph]*, 2022.
- [24] P. Koch, B. Muller, and J. Rafelski, “Strangeness in relativistic heavy ion collisions”, *Physics Reports*, vol. 142 167—262, 1986.
- [25] P. Gondolo and G. Gelmini, “Cosmic abundances of stable particles: Improved analysis”, *Nucl. Phys. B* 360 145, 1991.
- [26] M. Cannoni, “Exact theory of freeze-out”, *Eur. Phys. J. C* 75:106, 2015.
- [27] M. D. Schwartz, *Quantum Field Theory and the Standard Model*. Cambridge University Press, 2014.
- [28] T. Dougall and S. D. Wick, “Dirac magnetic monopole production from photon fusion in proton collisions”, *Eur. Phys. J. A* 39:213-217, 2009.
- [29] K. A. Milton, “Theoretical and experimental status of magnetic monopoles”, *Rept. Prog. Phys.* 69, 1637, 2006.
- [30] G. R. Kalbfleisch, K. A. Milton, M. G. Strauss, L. Gamberg, E. H. Smith, and W. Luo, “Improved experimental limits on the production of magnetic monopoles”, *Phys. Rev. Lett.* 85, 5292, 2000.
- [31] L. Epele, H. Fanchiotti, C. Canal, V. Mitsou, and V. Vento, “Looking for magnetic monopoles at lhc with diphoton events”, *Eur. Phys. J. Plus* 127, 60, 2012.
- [32] G. Aad and others (ATLAS Collaboration), “Search for magnetic monopoles $\sqrt{s} = 7$ tev in pp collisions with the atlas detector”, *Phys. Rev. Lett.* 109, 261803, 2012.

- [33] M. Collaboration,
- [34] W. Florkowski, *Phenomenology of Ultra-relativistic Heavy-ion Collisions*. World Scientific, 2010.
- [35] W. Busza, K. Rajagopal, and W. van der Schee, “Heavy ion collisions: The big picture and the big questions”, *Annu. Rev. Nucl. Part. Sci.*, vol. 68:339–76, 2018.
- [36] K. Yagi, T. Hatsuda, and Y. Miake, *Quark-Gluon Plasma: From Big Bang to Little Bang*. Cambridge University Press, 2005.
- [37] M. Maggiore, *A Modern Introduction to Quantum Field Theory*. Oxford University Press, 2005.
- [38] L. Abreu, F. Navarra, M. Nielsen, and H. Vieira, “Interactions of the doubly charmed state T_{cc}^+ with a hadronic medium”, *Eur. Phys. J. C*, vol. 82, 296, 2022.
- [39] A. D. Dolgov and Y. B. Zeldovich, “Cosmology and elementary particles”, *Rev. Mod. Phys.* 53, 1, 1981.
- [40] A. Tawfik and E. Abbas, “Thermal description of particle production in au-au collisions at rhic energies (star)”, *Phys. Part. Nuclei Lett.* 12, 521–531, 2015.
- [41] R. Workman *et al.*, “Review of particle physics”, *Particle Data Group*, 2022.
- [42] M. Cannoni, “Relativistic and nonrelativistic annihilation of dark matter: A sanity check using an effective field theory approach”, *The European Physical Journal C* 76, 2016.
- [43] B. Ryden, *Introduction to Cosmology*. Cambridge University Press, 2006.
- [44] E. W. Kolb and M. S. Turner, *The Early Universe*. Addison-Wesley Publishing Company, 1990.
- [45] B. W. Lee and S. Weinberg, “Cosmological lower bound on heavy-neutrino masses”, *Phys. Rev. Lett.* 39, 165, 1977.
- [46] S. Arunasalama and A. Kobakhidze, “Electroweak monopoles and the electroweak phase transition”, *Eur. Phys. J. C (2017)* 77:444, 2017.

Appendices

Appendix A

Definitions

We adopt the SI natural units:

$$c = \epsilon_0 = \hbar = 1$$

We assume the Einstein notation:

$$x_i y_i = \sum_i x_i y_i$$

and indices written with the Greek alphabet take on values $(0, 1, 2, 3)$ while the Latin alphabet take on values $(1, 2, 3)$.

The Minkowski metric $\eta^{\mu\nu}$ is:

$$\eta^{\mu\nu} = \begin{pmatrix} 1 & 0 & 0 & 0 \\ 0 & -1 & 0 & 0 \\ 0 & 0 & -1 & 0 \\ 0 & 0 & 0 & -1 \end{pmatrix} \quad (\text{A.1})$$

which is symmetric:

$$g^{\mu\nu} = g^{\nu\mu},$$

and defines the operations of raising and lowering indices:

$$\begin{aligned} V^\mu &= g^{\mu\nu} V_\nu \\ V_\mu &= g_{\mu\nu} V^\nu. \end{aligned} \quad (\text{A.2})$$

The four-momentum is denoted by $p^\mu = (E, \mathbf{p})$ and the inner product is:

$$p_1 \cdot p_2 = E_1 E_2 - \mathbf{p}_1 \cdot \mathbf{p}_2 = E_1 E_2 - p_1 p_2 \cos \theta, \quad (\text{A.3})$$

begin θ the angle between \mathbf{p}_1 and \mathbf{p}_2 .

In the center of mass frame we have for the quarks (q) and monopoles (p):

$$\begin{aligned} E_{q_1} &= E_{q_2} \\ E_{p_1} &= E_{p_2} \\ E_{q_i} &= E_{p_i} = E. \end{aligned} \tag{A.4}$$

Consequently

$$\begin{aligned} q_1 \cdot p_1 &= E^2 - qp \cos \theta = q_2 \cdot p_2 \\ q_1 \cdot p_2 &= E^2 + qp \cos \theta = q_2 \cdot p_1 \\ q_1 \cdot q_2 &= E^2 + q^2 = E^2 + m_q^2 \\ p_1 \cdot p_2 &= E^2 + p^2 = E^2 + m_p^2, \end{aligned} \tag{A.5}$$

for $q^2 = m_q^2$ and $p^2 = m_p^2$. The Mandelstam variables are defined:

$$\begin{aligned} t &= (q_1 - p_1)^2 = m_q^2 + m_p^2 - 2q_1 p_1 = (-q_2 + p_2)^2 = m_q^2 + m_p^2 - 2q_2 p_2 \\ u &= (q_1 - p_2)^2 = m_q^2 + m_p^2 - 2q_1 p_2 = (-q_2 + p_1)^2 = m_q^2 + m_p^2 - 2q_2 p_1 \\ s &= (p_1 + p_2)^2 = (q_1 + q_2)^2 \\ s + t + u &= \sum_{i=1}^4 m_i^2, \end{aligned} \tag{A.6}$$

where m_i are the masses of the particles in the initial and final states.

The spinor sum rules is:

$$\begin{aligned} \sum_s u_s(p) \bar{u}_s(p) &= (\not{p} + m) \\ \sum_r \bar{v}_r(p) v_r(p) &= (\not{p} - m), \end{aligned} \tag{A.7}$$

where $\not{p} = \gamma^\mu p_\mu$. The properties of Dirac's matrix is:

$$\begin{aligned} \text{Tr}[\gamma^\mu \gamma^\nu] &= 4\eta^{\mu\nu} \\ \text{Tr}[\gamma^\mu \gamma^\nu \gamma^\sigma \gamma^\rho] &= 4\eta^{\mu\nu} \eta^{\sigma\rho} - 4\eta^{\mu\sigma} \eta^{\nu\rho} + 4\eta^{\mu\rho} \eta^{\nu\sigma}, \end{aligned} \tag{A.8}$$

and

$$\begin{aligned} \text{Tr}[(u_s \gamma^\mu \bar{u}_s)(\bar{v}_r \gamma^{\mu'} v_r)] &= \text{Tr}[(\not{p} + m) \gamma^\mu (\not{p} - m) \gamma^{\mu'}] \\ &= p_{1\rho} p_{2\sigma} (4\eta^{\mu\sigma} \eta^{\mu'\rho} - 4\eta^{\mu\mu'} \eta^{\sigma\rho} \\ &\quad + 4\eta^{\mu\rho} \eta^{\mu'\sigma}) - 4m^2 \eta^{\mu\mu'}. \end{aligned} \tag{A.9}$$

The angular differential cross section is:

$$\frac{d\sigma}{d\Omega} = \frac{1}{64\pi^2 s} \frac{|\vec{p}_1|}{|\vec{q}_1|} |\overline{\mathcal{M}}|^2. \tag{A.10}$$

Now some Feynman rules and definitions useful to the calculations in next appendix.

- Incoming quark

$$\begin{array}{c} \longrightarrow \\ p \rightarrow \end{array} = u_s(p)c_i, \quad (\text{A.11})$$

- Outgoing quark

$$\begin{array}{c} \longrightarrow \\ p \rightarrow \end{array} = \bar{u}_s(p)c_i^\dagger, \quad (\text{A.12})$$

- Incoming antiquark

$$\begin{array}{c} p \rightarrow \\ \longleftarrow \end{array} = \bar{v}_s(p)c_i^\dagger, \quad (\text{A.13})$$

- Outgoing antiquark

$$\begin{array}{c} p \rightarrow \\ \longleftarrow \end{array} = v_s(p)c_i. \quad (\text{A.14})$$

where c_i refers to the three color charges of quarks and $i = 1, 2, 3$, with the hermitian column matrix representation:

$$c_1 = \begin{pmatrix} 1 \\ 0 \\ 0 \end{pmatrix} \quad (\text{A.15})$$

$$c_2 = \begin{pmatrix} 0 \\ 1 \\ 0 \end{pmatrix} \quad (\text{A.16})$$

$$c_3 = \begin{pmatrix} 0 \\ 0 \\ 1 \end{pmatrix}, \quad (\text{A.17})$$

Appendix B

Calculation of the invariant amplitudes and cross sections

Here we will compute the squared matrix amplitude averaged over spins and colors for both scalar and fermionic monopole pair production showed in Eq.(2.13) and (2.21) to obtain its respective cross sections.

B.1 Scalar monopole pair production

Starting with scalars monopoles we have from Eq.(2.12):

$$\begin{aligned}\mathcal{M}_{DY}^{(S=0)} &= u_s(q_1)c_i(-iQe\gamma_\mu)\bar{v}_s(q_2)c_i^\dagger\left(\frac{-i\eta^{\mu\nu}}{k^2}\right)(-ig)(p_{1\nu}-p_{2\nu}) \\ \mathcal{M}_{DY}^{*(S=0)} &= (p_{1\nu'}-p_{2\nu'})(ig)\left(\frac{i\eta^{\mu'\nu'}}{k^2}\right)v_{s'}(q_2)c_{i'}(iQe\gamma_{\mu'})\bar{u}_{s'}(q_1)c_{i'}^\dagger,\end{aligned}\tag{B.1}$$

where $\mathcal{M}_{DY}^{(S=0)}$ and $\mathcal{M}_{DY}^{*(S=0)}$ are the total matrix amplitude and its hermitian conjugate, respectively. Remembering that $u_s(q_1)$ and $\bar{v}_s(q_2)$ are the quark/anti-quark spinors dependent on the momentum q_1 and q_2 , respectively; c_i and c_i^\dagger the column matrix representing the three color charge of quarks given by Eq. (A.15), (A.16) and (A.17); Q is the fraction electric charges of quarks and e the positron charge; γ_μ the Dirac's matrix; $\eta^{\mu\nu}$ the Minkowski metric; p_1 and p_2 are the momentum of outgoing scalar monopoles; k is the photon momentum. The momentum dependence of spinors will be omitted for a clear notation from now on. Then, squaring Eq.(B.1) and summing over spins and colors, we have

$$\begin{aligned}|\mathcal{M}_{DY}^{S=0}|^2 &= \sum_{i,i'} \sum_{s,s'} \mathcal{M}_{DY}^{(S=0)} \mathcal{M}_{DY}^{*(S=0)} \\ &= \frac{e^2 g^2}{k^4} \left(\frac{2!}{4}\right) \left(\frac{1}{3}\right) \sum_Q Q^2 \sum_{i,i'} \sum_{s,s'} [u_s c_i \gamma_\mu \bar{v}_s c_i^\dagger \eta^{\mu\nu} (p_{1\nu} - p_{2\nu})] [(p_{1\nu'} - p_{2\nu'}) \\ &\quad \times \eta^{\mu'\nu'} v_{s'} c_{i'} \gamma_{\mu'} \bar{u}_{s'} c_{i'}^\dagger],\end{aligned}$$

the $2!$, $\frac{1}{4}$, $\frac{1}{3}$ factors account for the symmetry factor of the final states, and the averaging over spins and color states. The sum over the quark charges is

$$\sum_Q Q^2 = \left(\frac{1}{3}\right)^2 + \left(\frac{2}{3}\right)^2 = \frac{5}{9}$$

Then

$$\begin{aligned} |\mathcal{M}_{DY}^{S=0}|^2 &= \frac{5}{9} \frac{e^2 g^2}{k^4} \left(\frac{1}{6}\right) \sum_{i,i'} [c_i c_i^\dagger c_{i'} c_{i'}^\dagger] \sum_{s,s'} [(u_s \gamma_\mu \bar{v}_s) \eta^{\mu\nu} (p_{1\nu} - p_{2\nu})] [(p_{1\nu'} - p_{2\nu'}) \\ &\quad \times \eta^{\mu'\nu'} (v_{s'} \gamma_{\mu'} \bar{u}_{s'})] \\ &= \frac{5}{9} \frac{e^2 g^2}{k^4} \left(\frac{1}{6}\right) 3 \sum_{s,s'} [(u_s \gamma_\mu \bar{v}_s) (v_{s'} \gamma_{\mu'} \bar{u}_{s'})] \eta^{\mu\nu} (p_{1\nu} - p_{2\nu}) (p_{1\nu'} - p_{2\nu'}) \eta^{\mu'\nu'} \\ &= \frac{5}{9} \frac{e^2 g^2}{k^4} \left(\frac{1}{2}\right) \text{Tr}[(u_s \gamma_\mu \bar{v}_s) (v_{s'} \gamma_{\mu'} \bar{u}_{s'})] \eta^{\mu\nu} (p_{1\nu} - p_{2\nu}) (p_{1\nu'} - p_{2\nu'}) \eta^{\mu'\nu'}, \end{aligned} \quad (\text{B.2})$$

where we used from (A.15), (A.16) and (A.17):

$$\sum_{i,i'} [c_i c_i^\dagger c_{i'} c_{i'}^\dagger] = 3.$$

With the relation (A.9) the Eq. (B.2) becomes:

$$\begin{aligned} |\mathcal{M}_{DY}^{S=0}|^2 &= \frac{5}{9} \left(\frac{3e^2 g^2}{2k^4}\right) [q_1^\rho q_2^\sigma (4\eta_{\mu\sigma} \eta_{\mu'\rho} - 4\eta_{\mu\mu'} \eta_{\sigma\rho} + 4\eta_{\mu\rho} \eta_{\mu'\sigma}) - 4m^2 \eta_{\mu\mu'}] \\ &\quad \times (p_1^\mu - p_2^\mu) (p_1^{\mu'} - p_2^{\mu'}) \\ &= \frac{5}{9} \left(\frac{3e^2 g^2}{2k^4}\right) [4q_{1\mu} q_{2\mu} - 4q_1^\rho q_{2\rho} \eta_{\mu\mu'} + 4q_{1\mu} q_{2\mu'} + 4m^2 \eta_{\mu\mu'}] \\ &\quad \times (p_1^\mu p_1^{\mu'} - p_1^\mu p_2^{\mu'} - p_2^\mu p_1^{\mu'} + p_2^\mu p_2^{\mu'}), \end{aligned} \quad (\text{B.3})$$

where the factor 3 in the numerator introduces the contribution of three flavors of quarks. The properties (A.2) provide us:

$$\begin{aligned} |\mathcal{M}_{DY}^{S=0}|^2 &= \frac{5}{9} \left(\frac{3e^2 g^2}{2k^4}\right) [(4q_{1\mu} q_{2\mu} p_1^\mu p_1^{\mu'} - 4q_{1\mu} q_{2\mu} p_1^\mu p_2^{\mu'} - 4q_{1\mu} q_{2\mu} p_2^\mu p_1^{\mu'} + 4q_{1\mu} q_{2\mu} p_2^\mu p_2^{\mu'}) \\ &\quad + 4m^2 (p_{1\mu} p_1^{\mu'} - p_{1\mu} p_2^{\mu'} - p_{2\mu} p_1^{\mu'} + p_{2\mu} p_2^{\mu'}) \\ &\quad + (4q_{1\mu} q_{2\mu'} p_1^\mu p_1^{\mu'} - 4q_{1\mu} q_{2\mu'} p_1^\mu p_2^{\mu'} - 4q_{1\mu} q_{2\mu'} p_2^\mu p_1^{\mu'} + 4q_{1\mu} q_{2\mu'} p_2^\mu p_2^{\mu'}) \\ &\quad + 4m^2 (p_{1\mu} p_1^{\mu'} - p_{1\mu} p_2^{\mu'} - p_{2\mu} p_1^{\mu'} + p_{2\mu} p_2^{\mu'})]. \end{aligned}$$

Working at the center of mass frame follow the development using the relations (A.4) and (A.5):

$$\begin{aligned}
|\mathcal{M}_{DY}^{S=0}|^2 &= \frac{5}{3} \left(\frac{e^2 g^2}{2k^4} \right) 4 \{ (E^2 - pq \cos \theta)(E^2 + pq \cos \theta) - (E^2 + pq \cos \theta)(E^2 + pq \cos \theta) \\
&\quad - (E^2 - pq \cos \theta)(E^2 - pq \cos \theta) + (E^2 + pq \cos \theta)(E^2 - pq \cos \theta) \\
&\quad + 2m^2[p^2 - E^2 - p^2 + E^2 + p^2 + p^2] + (E^2 - pq \cos \theta)(E^2 + pq \cos \theta) \\
&\quad - (E^2 - pq \cos \theta)(E^2 - pq \cos \theta) - (E^2 + pq \cos \theta)(E^2 + pq \cos \theta) \\
&\quad + (E^2 + pq \cos \theta)(E^2 - pq \cos \theta) \},
\end{aligned}$$

which can be rewritten as

$$\begin{aligned}
|\mathcal{M}_{DY}^{S=0}|^2 &= \frac{5}{3} \left(\frac{e^2 g^2}{2k^4} \right) 4 [4(E^2 - pq \cos \theta)(E^2 + pq \cos \theta) - 2(E^2 + pq \cos \theta)(E^2 + pq \cos \theta) \\
&\quad - 2(E^2 - pq \cos \theta)(E^2 - pq \cos \theta) + 2m^2 p^2 + 2m^2 p^2],
\end{aligned}$$

and after some calculations we have

$$|\mathcal{M}_{DY}^{S=0}|^2 = \frac{5}{3} \left(\frac{e^2 g^2}{2k^4} \right) 32[p^2 q^2 - p^2 q^2 \cos \theta].$$

Writing the boosts

$$\begin{aligned}
\beta_q &= \frac{q}{E} \\
\beta_p &= \frac{p}{E}
\end{aligned}$$

and using the momentum conservation at vertex we can write the photon momentum in terms of the total energy E :

$$k^2 = (q_1 + q_2)^2 = (p_1 + p_2)^2 = (2E)^2 = 4E^2$$

then

$$\begin{aligned}
|\mathcal{M}_{DY}^{S=0}|^2 &= \frac{5}{3} \left(\frac{e^2 g^2}{32E^4} \right) 32E^4 [\beta_q^2 \beta_p^2 - \beta_q^2 \beta_p^2 \cos^2 \theta] \\
&= \frac{5}{3} (e^2 g^2) [\beta_q^2 \beta_p^2 - \beta_q^2 \beta_p^2 \cos^2 \theta].
\end{aligned}$$

It's important to note that the magnitude of the masses of quarks is comprehended in the range $10^{-6} \text{ TeV} \leq m \leq 10^{-3} \text{ TeV}$ (where the lower and upper limit are the mass of lightest and heavier quarks, respectively, according [41]) which is negligible compared with the monopole masses that in this work is $0.5 \text{ TeV} \leq M \leq 5 \text{ TeV}$. Considering $M \gg m$, the contribution of the boost β_q becomes insignificant compared with β_p . Hence $\beta_q \rightarrow 1$ and we define $\beta_p \equiv \beta$. We get

$$|\mathcal{M}_{DY}^{S=0}|^2 = \frac{5}{3} (e^2 g^2) \beta^2 [1 - \cos^2 \theta]. \quad (\text{B.4})$$

Using this result as input in the Eq. (A.10) we can compute the differential cross section:

$$\begin{aligned}\frac{d\sigma^{(S=0)}}{d\Omega} &= \frac{1}{64\pi^2 s} \frac{|\vec{p}_1|}{|\vec{q}_1|} \left\{ \frac{5}{3} (e^2 g^2) \beta^2 [1 - \cos^2 \theta] \right\} \\ &= \frac{\alpha_g \alpha_e}{4s} \frac{\beta_p}{\beta_q} \frac{5}{3} \beta^2 [1 - \cos^2 \theta],\end{aligned}$$

where Eq. (2.16) were used. Finally, we have

$$\begin{aligned}\frac{d\sigma^{(S=0)}}{d\Omega} &= \frac{5\alpha_g \alpha_e}{12s} \beta^3 [1 - \cos^2 \theta] \\ &= \frac{5\alpha_g \alpha_e}{12s} \beta^3 \sin^2 \theta.\end{aligned}\tag{B.5}$$

The usual definition for the infinitesimal solid angle is $d\Omega = \sin \theta d\theta d\phi$. So, the total cross section is given by

$$\sigma_{q\bar{q} \rightarrow M\bar{M}}^{(S=0)}(s) = \frac{5\alpha_g \alpha_e}{12s} \beta^3 \int_0^{2\pi} d\phi \int_0^\pi (\sin^2 \theta) \sin \theta d\theta,\tag{B.6}$$

which provides the Eq. (2.15). It is important to mention here that the monopole mass is much bigger than quarks masses, and then we do not distinguish the mass of the different flavor of quarks.

B.2 Fermionic monopole pair production

Now we have to follow the same steps in order to compute the squared matrix amplitude an the cross section for spin-1/2 monopole production. From Eq. (2.20) we have:

$$\begin{aligned}\mathcal{M}_{DY}^{(S=1/2)} &= u_s c_i (-iQe\gamma_\mu) \bar{v}_s c_i^\dagger \left(\frac{-i\eta^{\mu\nu}}{k^2} \right) a_r (-ig\gamma_\nu) \bar{b}_r \\ \mathcal{M}_{DY}^{*(S=1/2)} &= b_{r'} (ig\gamma_{\nu'}) \bar{a}_{r'} \left(\frac{i\eta^{\mu'\nu'}}{k^2} \right) v_{s'} c_{i'} (iQe\gamma_{\mu'}) \bar{u}_{s'} c_{i'}^\dagger,\end{aligned}\tag{B.7}$$

which follows

$$\begin{aligned}|\mathcal{M}_{DY}^{S=1/2}|^2 &= \sum_{i,i'} \sum_{s,s'} \sum_{r,r'} \mathcal{M}_{DY}^{(S=1/2)} \mathcal{M}_{DY}^{*(S=1/2)}, \\ |\mathcal{M}_{DY}^{S=1/2}|^2 &= \frac{e^2 g^2}{k^4} \left(\frac{1}{4} \right) \left(\frac{1}{3} \right) \sum_Q Q^2 \sum_{i,i'} \sum_{s,s'} \sum_{r,r'} [u_s c_i \gamma_\mu \bar{v}_s c_i^\dagger \eta^{\mu\nu} a_r \gamma_\nu \bar{b}_r] \\ &\quad \times [b_{r'} \gamma_{\nu'} \bar{a}_{r'} i\eta^{\mu'\nu'} v_{s'} c_{i'} \gamma_{\mu'} \bar{u}_{s'} c_{i'}^\dagger] \\ &= \frac{5 e^2 g^2}{9 k^4} \frac{1}{12} \sum_{i,i'} [c_i c_i^\dagger c_{i'} c_{i'}^\dagger] \sum_{s,s'} \sum_{r,r'} [u_s \gamma_\mu \bar{v}_s \eta^{\mu\nu} a_r \gamma_\nu \bar{b}_r] \\ &\quad \times [b_{r'} \gamma_{\nu'} \bar{a}_{r'} \eta^{\mu'\nu'} v_{s'} \gamma_{\mu'} \bar{u}_{s'}] \\ &= \frac{5 e^2 g^2}{36 k^4} \sum_{s,s'} \sum_{r,r'} [u_s \gamma_\mu \bar{v}_s \eta^{\mu\nu} a_r \gamma_\nu \bar{b}_r] [b_{r'} \gamma_{\nu'} \bar{a}_{r'} \eta^{\mu'\nu'} v_{s'} \gamma_{\mu'} \bar{u}_{s'}],\end{aligned}$$

$$|\mathcal{M}_{DY}^{S=1/2}|^2 = \frac{5e^2g^2}{36k^4} \text{Tr}[(u_s\gamma^\nu\bar{v}_s)(v_{s'}\gamma^{\nu'}\bar{u}_{s'})] \text{Tr}[(a_r\gamma_\nu\bar{b}_r)(b_{r'}\gamma_{\nu'}\bar{a}_{r'})].$$

So, using the relation A.9 and working at the center of mass frame, following the same steps that we performed for spin 0, we arrive at

$$|\mathcal{M}_{DY}^{S=1/2}(s, \theta)|^2 = \frac{e^2g^2}{3} [2 - \beta^2(1 - \cos^2 \theta)]. \quad (\text{B.8})$$

From where we can compute the differential cross section:

$$\begin{aligned} \frac{d\sigma^{(S=1/2)}}{d\Omega} &= \frac{1}{64\pi^2s} \frac{|\vec{p}_1|}{|\vec{q}_1|} \left\{ \frac{e^2g^2}{3} [2 - \beta^2(1 - \cos^2 \theta)] \right\} \\ &= \frac{\alpha_g\alpha_e}{12s} \frac{\beta_p}{\beta_q} [2 - \beta^2 \sin^2 \theta] \\ &= \frac{\alpha_g\alpha_e\beta}{12s} [2 - \beta^2 \sin^2 \theta]. \end{aligned}$$

Integrating over the solid angle we have

$$\sigma_{q\bar{q} \rightarrow M\bar{M}}^{(S=1/2)}(s) = \frac{\alpha_g\alpha_e\beta}{12s} \int_0^{2\pi} d\phi \int_0^\pi [2 - \beta^2 \sin^2 \theta] \sin \theta d\theta, \quad (\text{B.9})$$

and solving this integral we get the Eq. (2.22).